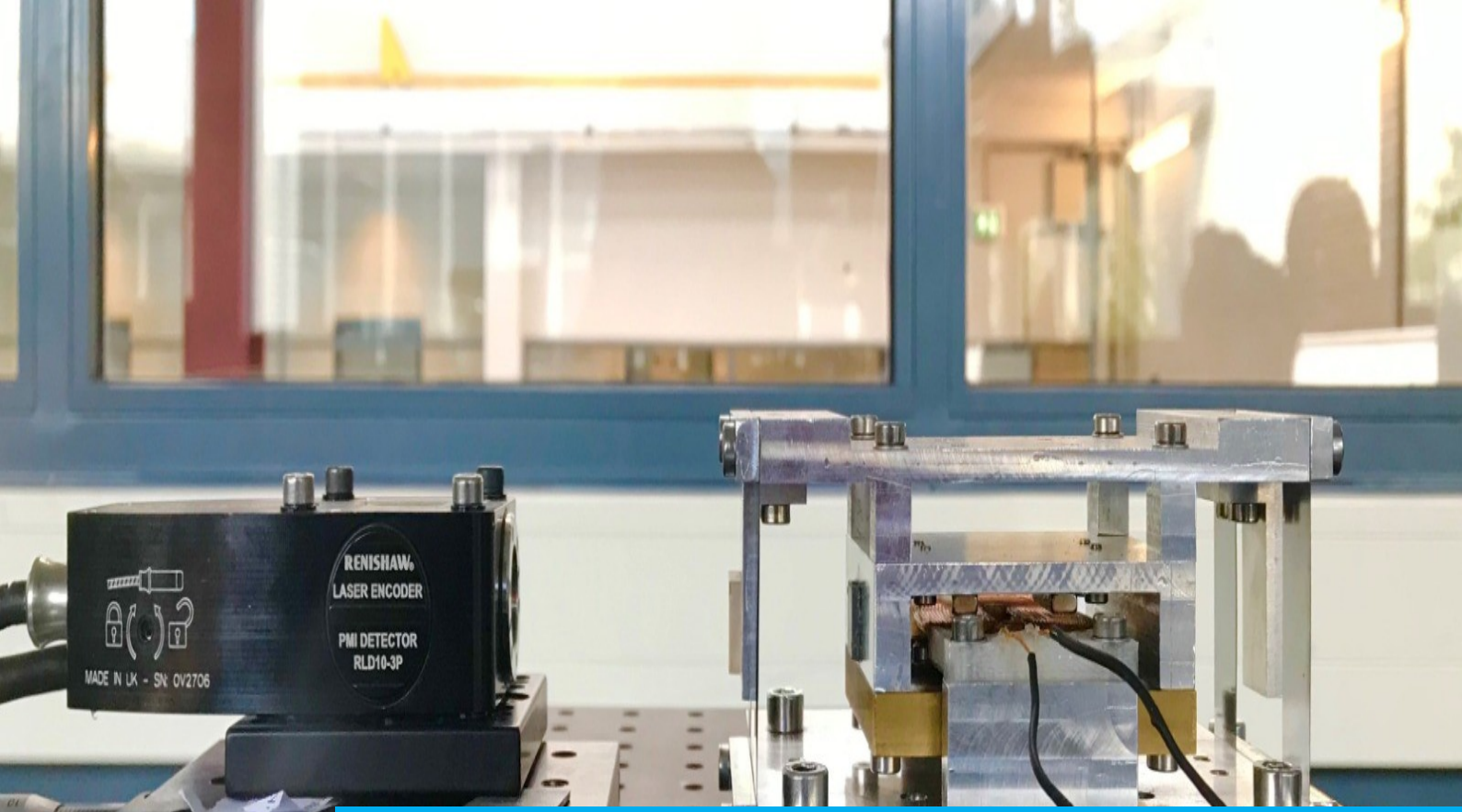

Department of Precision and Microsystems Engineering

Augmented Fractional-Order Reset Control: Application in Precision Mechatronics

Aldo Yonathan Sebastian

Report no : MSD 2020.026
Coach : Nima Karbasizadeh & Dr. N. Saikumar
Professor : Prof. S.H. HosseinNia
Specialisation : Mechatronic System Design
Type of report : Master Thesis
Date : August 19, 2020

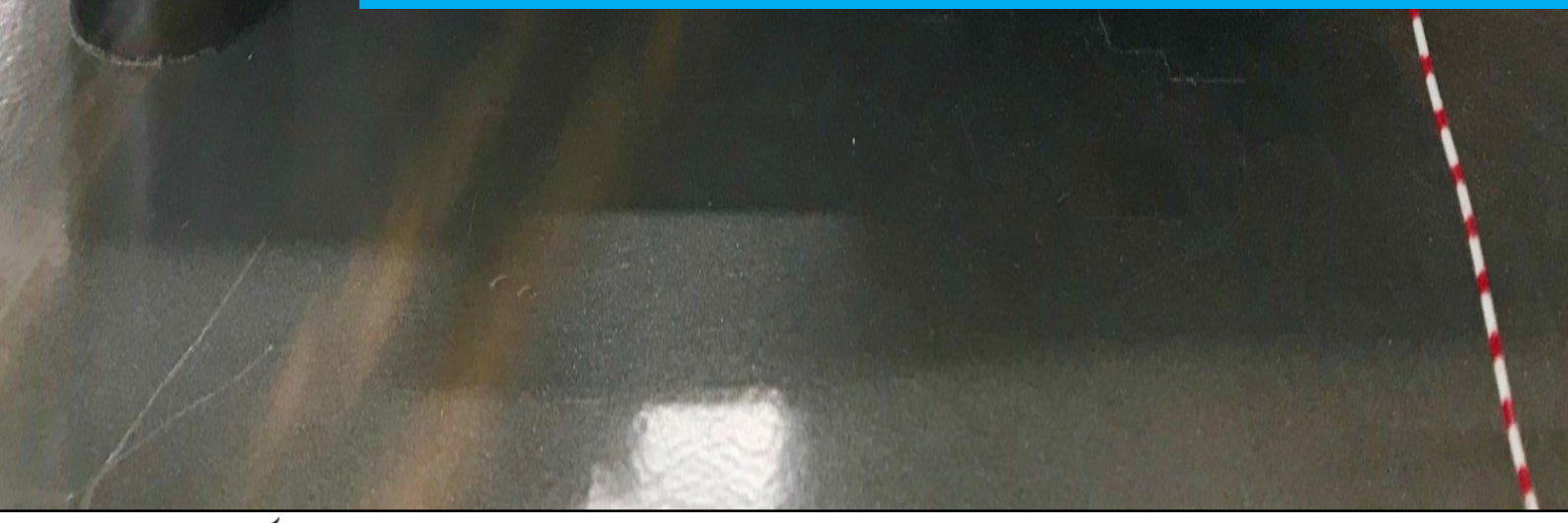

AUGMENTED FRACTIONAL-ORDER RESET CONTROL: APPLICATION IN PRECISION MECHATRONICS

by

Aldo SEBASTIAN

For the degree of Master of Science in Mechanical Engineering at Delft University of Technology

To be defended publicly on 19 August 2020 at 9 am

Student Number:	4787366
Supervisors:	Nima Karbasizadeh Eshafani
	Dr. Niranjan Saikumar
	Prof. S.H. HosseinNia
Thesis committee:	Dr. S.H. HosseinNia
	Dr. Niranjan Saikumar
	Dr.ir. J.F.L. Goosen
	Dr. Matin Jafarian
	N. Karbasizadeh MSc

An electronic version of this dissertation is available at
http://repository.tudelft.nl/.

TU Delft Delft University of Technology

PREFACE

I would like to thank my supervisors: Nima Karbasizadeh, Hassan HosseinNia Kani, and Niranjan Saikumar.

Nima Karbasizadeh, for helping me setting up and being very helpful, attentive and giving me ideas on what I should do. He always replies to my emails immediately and answered my doubts promptly. There has been a lot of instances where I am stuck with my code and he patiently went through the mess with me and helped me get unstuck. His knowledge on "tricks" in MATLAB, Simulink and LaTEX have saved me hours of trial and error; I thank him very much for his daily guidance and help.

Hassan HosseinNia, for giving me the project. I highly appreciate his concern and willingness to get highly involved in my thesis and paper even though he not my daily supervisor. Especially amid the pandemic, I really appreciate the long video calls, scrutinizing every detail of what I am doing and writing. He always reminded me to "have fun", which is something that I always forgot to do and what should've been my main motivation. Thank you for tolerating my endless mistakes in coding and being patient with my slow-learning self.

Niranjan Saikumar, for providing help with my experiment set-up and scrutinizing my paper as well to the smallest iota. Although he is not my main supervisor, I really thank him for the meetings I have with him, where he really challenged me with very difficult questions that I honestly couldn't answer. It has been a valuable lesson for me, to always be critical of what I read, results that I obtain or my MATLAB codes; to always ask why certain things happen and not just accept them the way they are and simply report them. It is the most important self-development point that I take away from this thesis experience, and I thank him for exposing this.

Ali Ahmadi Dastjerdi, for helping me with setting up the experiment. Thank you for spending a lot of time (sometimes up until the night) and always checking up on me even though you don't have to.

Jo Spronck and Andres Hunt, for organizing the Monday Meetings and exposing me to interesting engineering discussions. Thank you for your inputs on my presentation and how to improve myself.

All my fellow friends in the HTE department, for the good and bad things that we share and experience together. Thank you for your inputs which helped me, especially emotionally, through the thesis and also the whole Masters programme.

A.M.D.G

Aldo Sebastian
Delft, August 2020

CONTENTS

1

INTRODUCTION

From the invention of semiconductors in 1874 and the transistor in 1948 [1], the high-tech industry has drastically developed to meet the increasing need of electronics that has become more pivotal in the lives of the modern era. Such demand is currently met through production of semiconductors through a process called litography. Figure 1.1 shows a typical litography machine made by ASML, a leading company in the high-tech industry.

Figure 1.1: DUV Litography machine by ASML

The litography machines outputs semiconductors in bulk, in which each bulk is termed a waver. The motion of these wavers inside the machine requires precise control, which currently uses a control scheme called PID. PID is currently the workhorse of the industry, dominant in use due to its versatility and ease in tuning. However, the increasing need in rate of production requires the controllers to have a higher bandwidth and accu-

racy [2]. Due to the linear nature of PID, satisfying these requirements inevitably reduces the stability margin of the controller. This fundamental limitation presents itself mathematically through well-known relations such as the waterbed effect and Bode gain phase relation.

There have been attempts to circumvent this limitation through the use of nonlinear methods, however most of them are complex in nature and possess complicated tuning methods. Most importantly, they are not compatible with the loop shaping method, which utilizes the frequency response of the controller and what made PID highly attractive.

However, among these nonlinear methods, one of them called reset control has gained a lot of attention due to simplicity in tuning and compatibility with the loop shaping method [3], [4], [5], [6]. A typical reset element resets its state to zero whenever the input crosses zero. Clegg [7] applied the idea of reset to a linear integrator, with the Describing Function analysis [8] showing that the Clegg Integrator possesses a phase lag of $-38°$ instead of $-90°$ that a linear integrator has, while still maintaining the gain behaviour of the linear integrator. Such behaviour mean that the gain behavior of linear integrator can be exploited without a large inevitable reduction in stability, meaning that the aforementioned fundamental tradeoff that is charateristic of linear controllers is now reduced. The Clegg Integrator has been further developed to be incorporated in first order systems (termed First Order Reset Controller) and second order systems (termed Second Order Reset Controller), which extends the possibility of gaining the aforementioned benefit for more complex systems and controllers.

In spite of these promising results, the above benefit is often not seen in practice. This is because the Describing Function analysis neglects the higher order harmonics that is also output by the reset controller. Through the works of Cai [9], it was found that the sequence of parts that construct a reset controller has a significant effect on the contribution of the higher order harmonics in the output of the controller.

Cai's work is done through the framework of usage of the reset element within other control elements. Through his work and the work of Oustasloup et. al. [10], which utilizes fractional order calculus to develop an approximation for non-integer transfer functions, it is surmised that it might be possible to break a Clegg Integrator into fractional reset parts and find the optimal sequence and reset values of each part such that the influence of higher order harmonics is reduced. This thesis attempts to investigate this possibility, by investigating the behaviour of fractional order elements under reset and using an optimization routine to find the optimal reset values of the fractional parts. This would make the aforementioned benefit of a Clegg Integrator one step closer to be consistently realized in practice.

2

LITERATURE REVIEW

This chapter reviews the available literature within reset control in conference paper format. The preliminaries of reset control is first introduced. Then, limitations of reset control that prevent realization of benefits of reset control are explained. The final section elaborates different strategies to mitigate these limitations, with a concluding part that explains the significance of this thesis within the context of reset control.

Reset Control For Precision Motion Systems

Aldo Sebastian
High Tech Engineering, TU Delft

***Abstract*—In the motion control industry, PID (Proportional Integral Derivative) controller is highly favored due to its ease of implementation through the loop shaping method in frequency domain. However, there is an increasing need to obtain higher precision while maintaining the same robustness, which is impossible to achieve with PID control due to inherent limitations it possesses being that it is linear in nature. Reset controller is a class of nonlinear controller that has been successful in overcoming the fundamental limitation of PID controller while simultaneously being compatible with the loop shaping method, which is a feature that is not present in other nonlinear control schemes. However, reset control suffer from problems such as limit cycles and existence of higher order harmonics, which makes the expected increase in performance physically not realizable. This paper reviews the theory behind reset control, its shortcomings and possible strategies to overcome them.**

***Index Terms*—PID, Reset Control, Limit Cycle, Precision Systems, Higher Order Harmonics**

I. Introduction

ONE recent survey [1] indicates that among different control strategies, PID control still outperforms others in terms of adoption and usage in a wide range of industries, especially in the motion control industry [2] due to ease of tuning (e.g. using loop shaping method) and acceptable tradeoff between performance (specifically tracking and precision performance) and robustness. In spite of this, PID is still inherently a linear controller, which means it has fundamental limitations that causes a mandatory tradeoff between precision and robustness. These limitations are known as the Waterbed effect and Bode's gain phase relation [3]. Bode's gain phase relation demonstrates how the phase of a linear control element is dependent upon the slope of the gain by a fixed relation. The Waterbed effect shows how reducing the gain of the sensitivity function of a closed loop system at low frequencies in order to improve tracking and disturbance rejection performance has a consequence of increasing the peak of the function, which means that the stability level has been reduced. These two limitations show that there is a a fundamental trade-off between performance (tracking and noise rejection) and stability.

To reduce this tradeoff, one could resort to nonlinear control schemes. Reset control is one such option, where some or all of the states of the controller are reset to zero or a fraction of the current value given certain conditions. Reset control has been successfully implemented in a wide range of situations, such as controlling plants with large parametric uncertainty [4], improving hard-disk systems' mid-frequency disturbance rejection performance [5], and improving performance of servomotors by resetting fractional order integrators [6]. One particular attractive aspect of reset control is the availability of an approximate frequency response that utilizes a technique called Describing Function (DF), which makes loop shaping technique (that made PID control desireable) also applicable to reset control. This gives reset control an advantage over other nonlinear control alternatives.

The earliest and simplest reset controller is the Clegg Integrator (CI) that was introduced by Clegg in 1958 [7]. A CI is an integrator where its state resets to zero whenever its input is zero. In the frequency domain, the CI has a similar gain performance compared to a linear integrator, however it has a -38 degrees less phase lag compared to -90 of that of the linear integrator. This means that from a time domain perspective, a system controlled with a CI would have a lower overshoot, while from a frequency domain perspective the system would be further away from instability compared to if it is controlled with a linear integrator. Further application of reset control schemes include applying it to first and second order linear control elements (known as First Order Reset Element (FORE) and Second Order Reset Element (SORE) respectively), which introduces design variables that can be tuned to improve performance at desired range of frequencies.

Despite the advantages offered by reset control, the resetting action introduces unwanted dynamics in time domain response such as limit cycles. In addition, the nature of Describing Function being an approximation of the frequency response causes inaccurate results when used in closed-loop analysis. This literature review will address the various aspects of reset control, its shortcomings and current methods available to address this.

II. Reset Control

A. Definition

Reset control is a class of nonlinear controllers where some or all of the states of a linear controller is set to

zero or some fraction of its current state when a certain condition is met [8]. For instance, a reset controller that resets its states to a fraction A_ρ of its current state when the input $e(t)$ is 0 is shown in state space in equation (1)

$$\begin{cases} \dot{x}(t) = A_r x(t) + B_r e(t) & \text{if } e(t) \neq 0 \\ x(t^+) = A_\rho x(t) & \text{if } e(t) = 0 \\ u(t) = C_r x(t) + D_r e(t) \end{cases} \quad (1)$$

A_r,B_r,C_r and D_r are the state matrices of the base linear system, and A_ρ is the reset matrix. Specifically, A_ρ is a diagonal matrix, where if $x(t)$ comprises of multiple states, then each diagonal of A_ρ indicates the degree to which the corresponding state is being reset, from 0 being full reset to 1 being not reset at all.

B. Describing function

Since reset control is nonlinear, it inherently does not have a frequency response. Describing Function (DF) is a method to approximate the frequency response of a reset controller by taking the first harmonic of a Fourier series decomposition of the output, and dividing it with the input to the controller [3]. The most commonly used input to construct the DF is a sinusoidal input, giving the term SIDF (Sinusoidal Input Describing Function) to refer to this situation. As an example, the describing function for a reset element with reset condition $e(t) = 0$ is given by:

$$G(j\omega) = C_r (j\omega I - A_r)^{-1} (I + j\theta_D(\omega)) B_r + D_r \quad (2)$$

where

$$\begin{aligned} \theta_D(\omega) &\triangleq -\frac{2\omega^2}{\pi} \Delta(\omega) \left[\Gamma_D(\omega) - \Lambda^{-1}(\omega)\right] \\ \Delta(\omega) &\triangleq I + e^{\frac{\pi}{\omega} A_r} \\ \Lambda(\omega) &\triangleq \omega^2 I + A_r^2 \\ \Gamma_D(\omega) &\triangleq \Delta_D^{-1} A_\rho \Delta \Lambda^{-1} \\ \Delta_D(\omega) &\triangleq I + A_\rho e^{\frac{\pi}{\omega} A_r} \end{aligned}$$

C. Reset Systems Stability

For the reset condition $e(t) = 0$, there exists a condition that will ensure that a plant controlled by a reset controller in closed loop will be asymptotically stable [9].

Theorem 1: Assume a function $V : \mathbb{R}^n \to \mathbb{R}$ that is positive-definite, continuously differentiable, and radially unbounded such that

$$\dot{V}(x) := \left(\frac{\partial V}{\partial \mathrm{x}}\right)^T A_{cl}\mathrm{x} < 0 \qquad \text{if } \mathrm{x} \neq 0 \quad (3)$$

$$\Delta V(\mathrm{x}) := V(A_R\mathrm{x}) - V(\mathrm{x}) \leq 0 \qquad \text{if } \mathrm{x} \in M \quad (4)$$

where

$$M = \{\mathrm{x} \in \mathbb{R}^{n_p+n_r} : C_{cl}\mathrm{x} = 0, (I - A_R)\,\mathrm{x} \neq 0$$

A_{cl} and A_R are the closed loop A matrix and reset matrix respectively, and $\mathrm{x}=\begin{bmatrix} x_R \\ x_p \end{bmatrix}$ are the states of the reset controller and the plant. If a V exists such that 3) and (4) are satisfied, the reset system is asymptotically stable. This stability condition is called Lyapunov stability theorem for reset systems.

This stability theorem can be specialized for quadratic V i.e. V that satisfies $V(\mathrm{x}) = \mathrm{x}^T P \mathrm{x}$ where P is a positive definite function [9].

Theorem 2: Let there be a constant $\beta \in \mathbb{R}^{n_r \times 1}$ and $P_\rho \in \mathbb{R}^{n_r \times n_r}, P_\rho > 0$ such that the Lyapunov equation

$$P > 0, \quad A_{cl}^T P + P A_{cl} < 0 \quad (5)$$

$$B_0^T P = C_o \quad (6)$$

$$|\lambda(A_\rho e^{\frac{\pi}{\omega} A_r})| < 1 \quad (7)$$

has a solution for P, where

$$C_0 = \begin{bmatrix} \beta C_p & 0_{n_r \times n_{nr}} & P_p \end{bmatrix}, B_0 = \begin{bmatrix} 0_{n_r \times n_r} \\ 0_{n_{nr} \times n_r} \\ I_{n_r \times n_r} \end{bmatrix} \quad (8)$$

with n_r and n_{nr} are the amount of resetted and non resetted states of the controller respectively, and C_p has size $1 \times n_p$ with n_p being the number of plant states. This criterion, however, only indicates whether the system is stable or not, and does not give an indication to the degree of stability of the system.

III. Examples of Reset Controllers

As alluded to in section I, reset controllers are basically common linear elements that are modified to reset their states when their inputs are zero [9]. This section elaborates the use of reset in more detail for some common linear controllers.

A. Clegg Integrator (CI)

The Clegg Integrator is an integrator whose state resets to 0 whenever the input is 0. The parameters in equation 1 become

$$A_r = 0, B_r = 1, C_r = 1, D_r = 0, A_\rho = 0$$

Figure 1 shows the frequency response of CI approximated using the Describing Function method. As seen from the figure, the phase lag of CI is -38.1°. Comparing to a linear integrator, CI has a similar gain behaviour but a much more reduced phase lag. This means that the CI will contribute less in increasing possibility of instability in closed loop usage, as compared to a linear integrator.

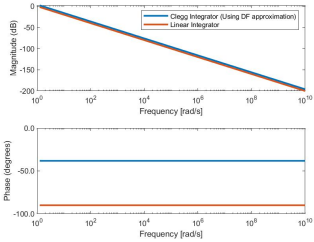

Fig. 1. Frequency response of a linear integrator vs. Clegg Integrator

B. First Order Reset Element (FORE)

The FORE is a first order low pass filter whose state is reset when the input is 0 [4]. The parameters of FORE in (1) are:

$$A_r = -\omega_r, B_r = \omega_r, C_r = 1, D_r = 0, A_\rho = 0 \quad (9)$$

where ω_r is the cutoff frequency of the filter. To include possibility of a partial reset, A_ρ can be modified to $\gamma \in [-1, 1]$. With partial reset, the FORE is known to be Generalized First Order Reset Element (GFORE). The describing function of this element, with partial reset, is:

$$G_{GFORE}(s) = \frac{1}{\frac{s}{\omega_r} + 1}\gamma \quad (10)$$

The plot of the describing function is shown in figure 2. From this figure, it is seen that the FORE ($\gamma = 0$) has less phase lag compared to a normal low pass filter with similar gain performance.

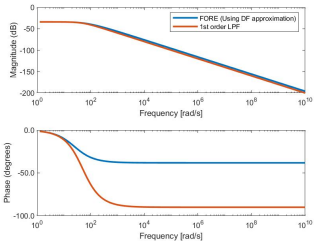

Fig. 2. Frequency response of 1st order LPF (Low Pass Filter) vs FORE, w_r=50 rad/s

C. SORE

The SORE is a second order LPF whose states are reset when the input is 0. The parameters in (1) are

$$A_r = \begin{bmatrix} 0 & 1 \\ -\omega_r^2 & -2\beta_r\omega_r \end{bmatrix}, B_r = \begin{bmatrix} 0 \\ \omega_r^2 \end{bmatrix} \quad (11)$$

$$C_r = \begin{bmatrix} 1 & 0 \end{bmatrix}, D_r = 0 \quad (12)$$

$$A_\rho = \begin{bmatrix} \gamma_1 & 0 \\ 0 & \gamma_2 \end{bmatrix} \quad (13)$$

where ω_r and β_r are the cutoff frequency and the damping ratio respectively, and for full reset γ_1 and γ_2 are zero. A_ρ is now a matrix instead of a scalar as was the case with CI and GFORE. This is because second order systems has two eigenvalues, which corresponds to two states. The describing function of SORE is:

$$GSORE(s) = \frac{1}{\left(\frac{s}{\omega_r}\right)^2 + \frac{2\beta_r s}{\omega_r} + 1}A_\rho \quad (14)$$

Figure 3 shows the plot of this Describing Function with full reset ($\gamma = 0$). With the existence of β_r, there is an extra tuning parameter available, giving more flexibility than FORE. It is observed in this figure that β_r controls the manner to which the phase drop occurs. It is also observed that for even low values of β_r (i.e. low damping) there's no appreciable resonance peak at ω_r, as would be the case with a linear second order LPF. This is advantageous since the tradeoff between a delayed phase drop and a consequently large resonance peak is now reduced.

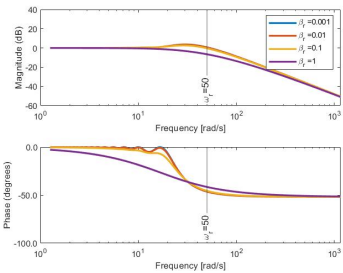

Fig. 3. Frequency response of SORE for different values of β_r

IV. Limitations of Reset control

A. DF Limitation

For the motion control industry, the advantages of reset control are primarily sought after in the frequency domain. However, when implementing the results in time domain, the expected benefits often do not occur. This is because the frequency response is approximated using the aforementioned Describing Function, where this method only takes into account the first harmonic of the output. Thus the use of loop shaping method by assuming the DF to be the frequency response of the reset element may produce incorrect conclusions [10].

To illustrate the issue, consider a Clegg Integrator controlling the second order plant

$$P(s) = 0.15\frac{s+2}{s^2+0.2s} \tag{15}$$

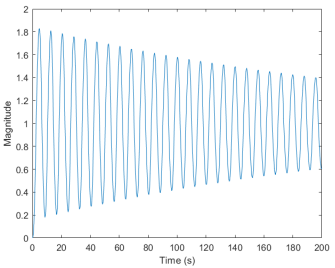

Fig. 4. Step response of CI controlling $\frac{0.15(s+2)}{(s^2+0.2s)}$

The frequency response of the open loop system using the Describing Function of CI is as shown in figure 5, with the step response shown in figure 4. We observe that frequency response predicts an unstable system, since the phase drops below -180 °at the crossover frequency. However, the step response shows a stable result. Thus loop shaping method cannot be fully trusted when using Describing Functions. This discrepancy is due to higher order harmonics that is present in the output, which is neglected by DF analysis.

Clearly the higher order harmonics of the output are significant. Nuij, and later by Kars [10] has developed a method to quantify the describing function of these higher order harmonics. These are called Higher Order

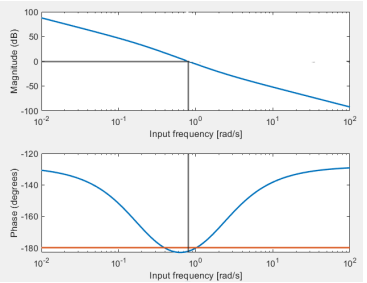

Fig. 5. Open Loop Frequency Response using Describing Function

Sinusoidal Input Describing Function (HOSIDF). The formula to find the HOSIDF is as shown:

$$G(j\omega) = \begin{cases} C_r\left(jwI - A_r\right)^{-1}\left(I + j\theta_p\left(a\right)\right)B_r + D_r & n = 1 \\ C_r\left(j\mu_n I - Ar\right)^{-1} j\theta_p\left(\omega\right)B_r & \text{for even } n \geq 2 \\ 0 \quad \text{for odd } n \geq 2 \end{cases}$$

The HOSIDF of the CI is shown in figure 6. Here it is observed that the higher order harmonics (non-blue color lines) have gain values that are close to that of the 1st harmonic (shown in blue line), which means that they are significantly inflencing the output of the CI.

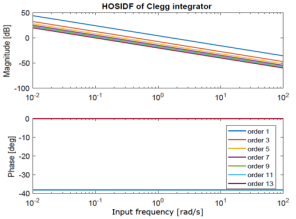

Fig. 6. HOSIDF of CI

It is desired to suppress these higher order harmonics so that the response of the system gets closer to resembling its describing function.

B. Unwanted Dynamics: Limit Cycle

Another problem that might occur with using reset controllers is unwanted dynamics caused by a phe-

nomenon called limit cycles [3]. To illustrate this problem, consider a plant $P(s) = \frac{1}{s+0.5}$ being controlled by a PCI (Proportional + Clegg Integrator) controller. The step response is shown in figure 7, compared with that of a PI controller. The system controlled by PCI indeed shows less overshoot due to the resetting action. However, there is a persistent oscillation at the set-point. To explain this, consider the control signal required to keep the response equal to setpoint. The final value theorem gives the steady state output of the closed loop system and the plant to be 1 and 2 respectively. This means that the control signal has to be a constant value of 0.5 in order to maintain the steady state output of the closed loop system. However, at steady state the error is 0, which means that the PCI will reset its state, causing the output of the controller to be 0 instead of 0.5, and thus the steady state condition is destabilized. The controller will then restabilize the output to setpoint, in which the destabilizing condition occurs again, causing a cycle referred to as limit cycle.

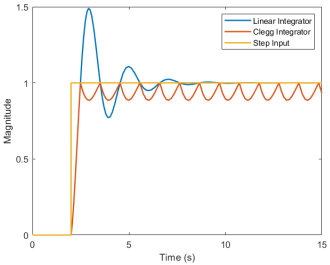

Fig. 7. Step response of $\frac{1}{s+0.5}$ controlled by Linear vs. Clegg Integrator

C. Impractical control signal

Consider the control signal output by the controller considered in section IV A, shown in figure 8. As can be seen there are jumps in the signal corresponding to the reset instants. This is undesirable for an actuator that has to physically realize this signal, since it is commanded to have a large change in its output in a very small time frame (essentially instantaneous). The actuator will have physical limitations in rate of change of output signal, and thus such a signal jump will not be realizable, causing time delays to the system which may reduce stability. In addition, subjecting the actuator to its physical limit (i.e. saturating it) multiple times will cause premature degradation of the life of the actuator.

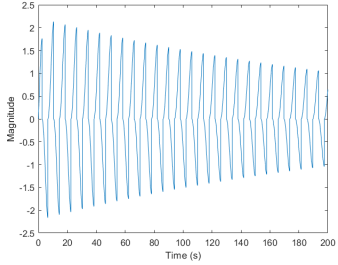

Fig. 8. Control signal of CI controlling $\frac{0.15(s+2)}{(s^2+0.2s)}$

D. Poor actual disturbance rejection

To obtain a better performance in terms of disturbance rejection an extra integrator is used with a PID controller to obtain a PI2D controller. However, this controller is still bound to the fundamental limitation of linear controller, with a consequently lower phase margin as the extra integrator is introduced. A Clegg Integrator can be added instead of a linear integrator to obtain the better disturbance rejection while reducing the negative consequence of reduced phase margin. Consider rejecting disturbance and noise of a second order plant, as shown in figure 9, with the Extra Controller block can be an extra linear integrator or extra Clegg Integrator. The bare PID controller is then tuned so that the open loop frequency response have a bandwidth of 100 Hz with a phase margin of 40 degrees, and then add an integrator or a Clegg Integrator and retune each of them so that the bandwidth is maintained at 100 Hz, as shown in figure 10. It should be kept in mind that the frequency response of the system with the Clegg Integrator is approximated using the describing function of the Clegg Integrator. A zoomed in plot of the phase plot of figure 9 is shown in figure 11. Indeed, PCIID gives a better phase margin compared to PI2D, while preserving the gain performance of PI2D.

However, applying a disturbance of 1 Hz in simulation shows the response shown in figure 12. The amplitude of the response of PCIID (in yellow), instead of matching that of PI2D (in red), exceeds it because of the jumping action. This jumping action is due to the higher order harmonics alluded to in subsection A of this section,

causing the response to not match that predicted by the open loop based on Describing Function.

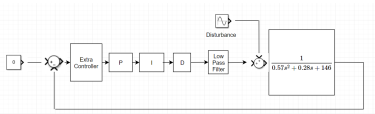

Fig. 9. Disturbance rejection scheme of plant: $\frac{1}{0.57s^2+0.28s+146}$

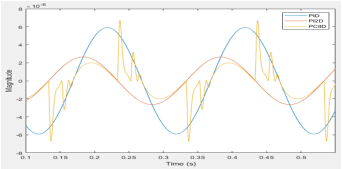

Fig. 12. Steady state response to 1 Hz disturbance from simulation

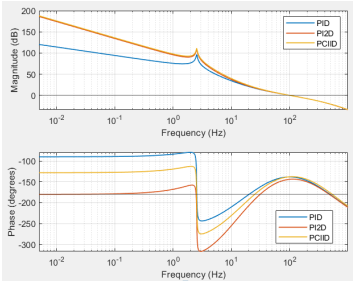

Fig. 10. Frequency response of $\frac{1}{0.57s^2+0.28s+146}$ controlled with various schemes

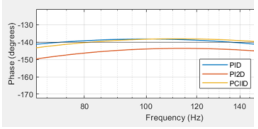

Fig. 11. Phase margin of $\frac{1}{0.57s^2+0.28s+146}$ controlled with various schemes

V. Reset Strategies to Overcome Limitations

Techniques that are available in literature to mitigate the aforementioned limitations will be outlined in this section.

A. Partial Reset

By applying different values to the diagonals of the reset matrix A_ρ (or to the value of γ in the case of CI and FORE), the magnitude of higher order harmonics will change. The value of γ, which builds the diagonal of A_ρ can vary between -1 and 1 to ensure Schur stability [11], meaning that the overall closed loop system will be internally stable. Figure 13 shows the step response of $\frac{1}{s+0.5}$ controlled with a partially reset controller. It is observed that the limit cycle problem is reduced, with the magnitude of the limit cycles reducing as the reset value is increased. This method also reduces the higher order harmonics, as seen in figure 15 where the 3rd order harmonic has a lower magnitude compared to full reset case. However, looking at the phase plot of figure 14, applying partial reset reduces the obtained phase lag reduction compared to full reset case. Therefore this strategy still involve a trade-off between provided increase in stability and actual performance of the element.

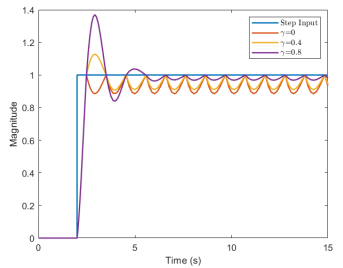

Fig. 13. Closed loop step response of $\frac{1}{s+0.5}$ controlled with partially reset Clegg Integrator

B. Reset with band

Instead of resetting the state of the controller to zero when the input is zero, reset with band strategy resets when the input instead enters a specified band B_δ [3]. δ, a real non-negative number, is the width of the band,

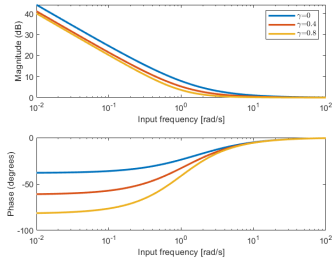

Fig. 14. Frequency response of $1/(s+0.5)$ controlled with partially reset Clegg Integrator, using describing function

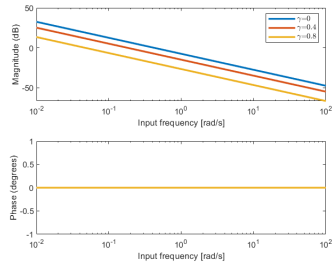

Fig. 15. Third order harmonic of $1/(s+0.5)$ controlled with partially reset Clegg Integrator

where the band is centered around zero. Mathematically this is defined as

$$\begin{cases} \dot{x}(t) = A_r x(t) + B_r e(t) & \text{if } (e(t), \dot{e}(t)) \neq B_\delta \\ x(t^+) = A_\rho x(t) & \text{if } (e(t), \dot{e}(t)) = B_\delta \\ u(t) = C_r x(t) + D_r e(t) \end{cases} \tag{16}$$

with

$$B_\delta = \{(e(t), \dot{e}(t)) \in \mathbf{R}^2 | (e(t) = -\delta \wedge \dot{e}(t) > 0) \vee (e(t) = \delta \wedge \dot{e}(t) < 0)\} \tag{17}$$

By tuning the value of δ, the problem of limit cycle is reduced. For instance, consider controlling the plant $\frac{1}{s+0.5}$ with a reset band CI. For $\delta = 0.34$, the limit cycle problem that was there with a standard CI is removed. However, it is found that this strategy requires careful tuning of δ. With a small reduction to $\delta = 0.33$, figure 16 shows that a very small limit cycle reoccurs, along with a steady state error. Particularly concerning is the observation that the transition back to the problematic steady state error condition as δ reduces is not gradual but rather abrupt. This makes the method not robust against model uncertainties and/or disturbances. Moreover, if δ is tuned to be too large in an attempt to achieve robustness, there will be less reset instants compared to traditional reset because as time elapses, the error signal will oscillate inside the band and so resetting does not occur anymore. This means that the system acts linearly and the advantages of reset is not fully realized.

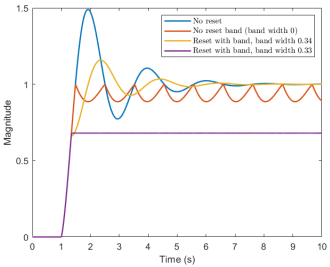

Fig. 16. Step response of $\frac{1}{s+0.5}$ controlled with reset band strategy

C. PI+CI

PI+CI controller is a parallel combination of a CI and a linear integrator [3]. There is an additional reset parameter p_{reset} that gives weight on the contribution of the CI and linear integrator on the output of the controller. p_{reset} can vary between 0 and 1, with a value of 0 and 1 making the integrating part of the PI+CI controller a completely linear one or a completely reset one respectively. PI+CI structure is shown in figure 17 and is represented by:

$$PI + CI = k_p(1 + \frac{1}{\tau_i}(\frac{1 - P_{reset}}{s} + \frac{P_{reset}}{\not{s}})) \tag{18}$$

Figure 18 shows the output of this scheme. Compared to partial reset strategy, it is shown that the limit cycle problem is significantly removed without adding any excessive overshoot. Clearly this strategy softens the

tradeoff between overshoot and limit cycles. In [12], Banos et. al. developed a tuning rule for the PI+CI controller, with [13] [14] showing examples of use of PI+CI controller in industrial applications.

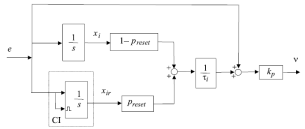

Fig. 17. PI+CI controller configuration

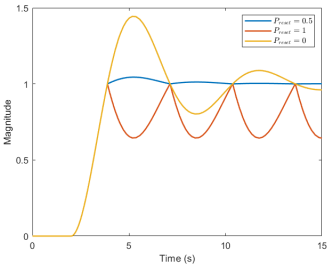

Fig. 18. Step response of $\frac{1}{s+0.5}$ controlled with PI+CI strategy

D. Placement of reset and linear elements

In motion control, reset element is often used to replace one of the elements that constitute a linear PID controller, or to complement a PID controller, which in combination makes a reset controller. For instance is a CgLp element developed by Saikumar et. al. [15], which when used in series with a PID controller produces a frequency response that has a very similar gain response as if the PID acts by itself, but with a larger phase lead at the bandwidth frequency. This controller is called a CgLp+PID controller. Yusuf [16] shows that different strategies used to tune the controller to achieve larger phase lead is still subject to an increase in influence of the higher order harmonics. Investigating this problem, Chengwei [17] found that sequence of components of a reset controller in tandem with linear controllers have an effect on the magnitude of the high order harmonics.

The linear part of a reset controller can be divided into lag and lead elements. The lag and lead elements is described as:

$$C_{lead}(s) = c_n s^n + c_{n-1} s^{n-1} + ... + c_0 s^0$$
$$C_{lag}(s) = \frac{1}{d_n s^n + d_{n-1} s^{n-1} + ... + d_0 s^0} \quad (19)$$

Chengwei found that the sequence with the reset element placed after a lead linear element and before a lag linear element gives the highest reduction in the magnitude of high order harmonics. This is because in this sequence, the lead element, which is an increasing function of frequency, does not have the chance to amplify higher order harmonics that is produced by the output of the reset part. In addition, placing the lag element at the end allows the generated higher order harmonics to be filtered, since the lag element is a decreasing function of frequency. Other possible sequences do not have both of these characteristics, which causes the higher order harmonics to be as effectively suppressed as this sequence. Figure 19 shows the magnitude of third order harmonic for different sequences of a first order lead and lag filter with a FORE. This optimal sequence was

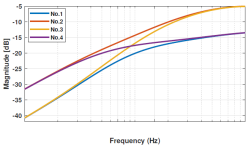

Fig. 19. Third harmonic of P(s) controlled with PID+FORE, with different sequences of the linear and nonlinear elements. No.1: Lead-Reset-Lag, No.2: Lag-Reset-Lead, No.3: Reset-Lead-Lag, No.4: Lead-Lag-Reset

analysed in closed loop configuration to validate the benefits, and indeed that is the case. Figure 20 shows the closed loop step response of a reset element consisting of linear PID controller and a FORE, controlling a second order mass spring damper system

$$P(s) = \frac{1}{1.077 \times 10^{-4} s^2 + 0.0049 s + 4.2218} \quad (20)$$

The lead-reset-lag sequence has the smallest settling time compared to other sequences. Also contrary to other sequences, this sequence has no steady state error and overshoot. In terms of precision performance, figure 21 shows the sensitivity function based on dividing the maximum of the error signal with the amplitude of a sinusoidal input, for different frequencies of the sinusoidal input. Again it is seen that the lead-reset-lag sequence has the lowest error for all frequencies.

Therefore this sequence is promising in making the DF more reliable in using loop shaping method for reset controllers.

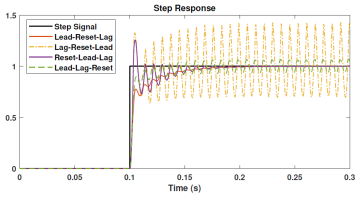

Fig. 20. Step response of P(s) controlled with PID+FORE, with different sequences of the linear and nonlinear elements

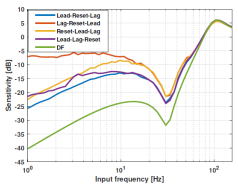

Fig. 21. Sensitivity function of P(s) controlled with PID+FORE, with different sequences of the linear and nonlinear elements. Here DF is the sensitivity function based on the describing function of PID+FORE, which is plotted here to show that it is inaccurate since it does not conform with the Lead-Reset-Lag curve, which is obtained numerically and so is more reflective of reality

VI. Conclusion

Linear controller such as PID is preeminently used in industry due to its robustness and ease of use through the loop shaping method. To meet the increasing need of improving linear controllers beyond its fundamental limitations, a class of nonlinear controllers known as reset control is highly attractive due to its ability to be tuned using loop shaping method by approximating its frequency response using the Describing Function, making the controller as simple to tune as linear controllers while having a better performance.

However, being inherently nonlinear, reset controllers do not produce sinusoidal outputs and thus its output contain Fourier higher order harmonics. The Describing Function method only incorporates the first harmonic, causing simulation or experimental results to deviate from expected theoretical results that was found by tuning the controller using loop shaping methods. Other problems include unwanted dynamics such as limit cycles.

Some methods have been proposed in literature to address the problem of limit cycles. Partial reset method can reduce the presence of higher order harmonics in the output, however it reduces the phase lead benefit simultaneously. In addition, limit cycles are not effectively removed compared to other methods such as PI+CI. Reset with band method is another promising method, however it only works for certain ideal plants and so is not robust against plant parameter uncertainties. In addition, it requires careful parameter tuning, in which a tuning rule is not yet present in literature.

Methods available in literature, as shown above, seem to be more focused in addressing limit cycle problems and are more preeminently validated in process systems (i.e. first order plants). To the best of the author's knowledge there exists no works in literature that address the problem of higher order harmonics in specific relation to the motion control industry. Works by Chengwei [17] has successfully attempted the use HOSIDF to reduce the effects of higher order harmonics. However this was addressed by analyzing the reset element in combination with other linear elements. It would be advantageous to reduce the higher order harmonics by examining the reset element by itself and changing the way it is implemented, making it more flexible to use in different situations.

References

[1] Yoshinori Shizuku et al. "A survey on industry impact and challenges thereof". In: *IEEE Control Systems* 37.1 (2017), pp. 17–18. ISSN: 1066033X. DOI: 10.1109/MCS.2016.2621438. URL: https://repository.tudelft.nl/islandora/object/uuid:5370c610-4112-49e9-b860-9d625d5b40c5?collection=educationhttps://ieeexplore.ieee.org/document/7823045.

[2] K. J. Åström and T. Hägglund. "The future of PID control". In: *Control Engineering Practice* (2001), pp. 1163–1175, 2001. ISSN: 09670661. DOI: 10.1016/S0967-0661(01)00062-4.

[3] Antonio Barreiro and Alfonso Bãnos. "Reset control systems". In: *RIAI - Revista Iberoamericana de Automatica e Informatica Industrial*. 2012. Chap. 1, pp. 11–17. DOI: 10.1016/j.riai.2012.09.007.

[4] Isaac Horowitz and Patrick Rosenbaum. "Nonlinear design for cost of feedback reduction in systems with large parameter uncertainty". In: *International Journal of Control* 21 (1975), pp. 977–

1001, 6 1975. ISSN: 13665820. DOI: 10.1080/00207177508922051.

[5] Yuqian Guo, Yuoyi Wang, and Lihua Xie. "Frequency-domain properties of reset systems with application in hard-disk-drive systems". In: *IEEE Transactions on Control Systems Technology* 17.6 (2009), pp. 1446–1453. ISSN: 10636536. DOI: 10.1109/TCST.2008.2009066.

[6] S. Hassan HosseinNia, Inés Tejado, and Blas M. Vinagre. "Fractional-order reset control: Application to a servomotor". In: *Mechatronics* 23.7 (2013), pp. 781–788. ISSN: 09574158. DOI: 10.1016/j.mechatronics.2013.03.005.

[7] J. C. Clegg. "A nonlinear integrator for servomechanisms". In: *Transactions of the American Institute of Electrical Engineers, Part II: Applications and Industry* (1958), pp. 41–42. ISSN: 0097-2185. DOI: 10.1109/tai.1958.6367399.

[8] Alfonso Banos, Joaquin Carrasco, and Antonio Barreiro. "Reset times-dependent stability of reset control systems". In: *2007 European Control Conference, ECC 2007*. 2007. ISBN: 9783952417386.

[9] Orhan Beker et al. "Fundamental properties of reset control systems". In: *Automatica* 40 (2004), pp. 905–915. ISSN: 00051098. DOI: 10.1016/j.automatica.2004.01.004.

[10] Kars Heinen. "Frequency analysis of reset systems containing a Clegg integrator". 2018. URL: https://repository.tudelft.nl/islandora/object/uuid{\%}3Accc37af2-fcbc-46ec-9297-afdc5c1ea4b5.

[11] T Yang. *Impulsive Control Theory*. 2001. ISBN: 354042296X. DOI: 10.1007/3-540-47710-1.

[12] Alfonso Banos and Angel Vidal. "Definition and tuning of a PI+CI reset controller". In: *2007 European Control Conference, ECC 2007*. 2007. ISBN: 9783952417386. DOI: 10.23919/ecc.2007.7068602.

[13] Alejandro Fernndez Villaverde et al. "Reset control for passive bilateral teleoperation". In: *IEEE Transactions on Industrial Electronics* (2011). ISSN: 02780046. DOI: 10.1109/TIE.2010.2077610.

[14] Alfonso Baños and Angel Vidal. "Design of PI+CI reset compensators for second order plants". In: *IEEE International Symposium on Industrial Electronics*. 2007. ISBN: 1424407559. DOI: 10.1109/ISIE.2007.4374584.

[15] Niranjan Saikumar, Duarte Valério, and S. Hassan HosseinNia. "Complex order control for improved loop-shaping in precision positioning". In: (2019), p. 3. arXiv: 1907.09249. URL: http://arxiv.org/abs/1907.09249.

[16] Y Salman. "Tuning a Novel Reset Element through Describing Function and HOSIDF Analysis". 2018. URL: https://repository.tudelft.nl/islandora/object/uuid{\%}3A2236e1f6-4dc5-4f7f-96da-fc83ead69445.

[17] Chengwei Cai et al. "The Optimal Sequence for Reset Controllers". 2019. URL: https://www.semanticscholar.org/paper/The-Optimal-Sequence-for-Reset-Controllers-by-Cai-Dastjerdi/ea0ac3b0d2868255e2107699a62b56cfe85b0d58.

[18] Yoshinori Shizuku and Yoshihisa Ishida. "Design of a PID controller based on a reset compensator using the Clegg integrator". In: *Proceeding - 2016 IEEE 12th International Colloquium on Signal Processing and its Applications, CSPA 2016*. 2016. ISBN: 9781467387804. DOI: 10.1109/CSPA.2016.7515807.

[19] L Hazeleger. "Second-Order Reset Elements for Improved Stage Control Design". In: (2015), pp. 14–18.

[20] Linda Chen. "Development of CRONE reset control". PhD thesis. 2017. URL: https://repository.tudelft.nl/islandora/object/uuid:5370c610-4112-49e9-b860-9d625d5b40c5?collection=education.

3

OBJECTIVE

3.1. PROBLEM DEFINITION

The literature review has shown how available methods in literature to address problems in reset control have been more focused on addressing issues pertaining to time domain, with validation being focused on first-order systems. Work by Cai [9] has successfully addressed the problems of reset control within frequency domain, through using HOSIDF tool by [8] to reduce higher order harmonics by finding the optimal sequence of reset controllers. Taking this idea of rearranging sequences of parts of reset controllers and the possibility of deconstruction of a reset element to fractional elements through works by Oustasloup et. al. [10] and recently by Hassan et. al. [5], the objective of this thesis is established:

Find the number of parts and the optimal reset values of each part of the fractional-order analogue of Clegg Integrator that results in the most minimum magnitude of the higher order harmonics while maintaining the benefits of the Clegg Integrator, and validate that the higher order harmonics reduction results in a better closed loop performance.

3.2. APPROACH

The approach taken to complete the objective is:

- Use HOSIDF to investigate the gain and phase behavior of a fractional reset integrator, and how the first harmonic gain and phase of the Clegg Integrator can be replicated faithfully by a collection of these fractional elements.
- Find the reset values of the elements that make up the fractional analogue such that the higher order harmonics are minimized using an optimization routine.
- Using the optimization results, recommend the best architecture that will be the most optimal fractional order analogue of the Clegg Integrator.

- Investigate the non-zero higher order harmonic phase of the fractional order analogue on possibility of further reducing the effects of higher order harmonics' influence on the output of the controller.
- Validate the fractional order analogue's superiority over the Clegg Integrator in closed loop through closed loop disturbance rejection control of a fine stage actuated by a Lorentz actuator.

4

AUGMENTED FRACTIONAL-ORDER RESET CONTROL: APPLICATION IN PRECISION MECHATRONICS

This chapter presents, in conference paper format, the description of the optimal architecture of augmented fractional analogue of Clegg Integrator. Firstly, the theory of reset control and Describing Function is revisited. Then, the equivalence of the Clegg Integrator and a proposed fractional order analogue of the Clegg Integrator is established through a mathematical derivation. This analogue is then modified such that it still pertains the same first harmonic performance as the Clegg Integrator, but with lower higher order harmonics. This is achieved through use of a constrained optimization routine. Finally, the expected benefit of use of the modified fractional order analogue is validated in closed loop simulation and experiment.

Augmented Fractional-order Reset Control: Application in Precision Mechatronics

Aldo Sebastian, Nima Karbasizadeh, Hassan HosseinNia, Niranjan Saikumar
High Tech Engineering, TU Delft

***Abstract*—Linear control such as PID possesses fundamental limitations, seen through the Waterbed effect. Reset control has been found to be able to overcome these limitations, while still maintaining the simplicity and ease of use of PID control due to its compatibility with the loop shaping method. However, the resetting action also gives rise to higher order harmonics that hinders consistent realization of the aforementioned expected improvement. In this paper, a fractional-order augmented state analogue of the reset integrator is investigated. This analogue is composed of a series of augmented states that each possess unique reset values, providing the same first order harmonic behavior but reduced higher order harmonics magnitude compared to the reset integrator. The optimal number of augmented states along with the corresponding tuning values are investigated. To validate the improvement, the reset integrator and the optimal fractional order analogue is tuned to equally improve disturbance rejection of a high precision 1 DOF positioning stage while maintaining the stability level, with both designed to overcome linear control. From simulation and experimental results, it was found that the novel fractional-order augmented state analogue gives rise to disturbance rejection performance that is closer to the desired and expected improvement, compared to using the traditional reset integrator.**

***Index Terms*—PID, Reset Control, Fractional Calculus, Fractional Order Control, Motion control, Higher Order Harmonics**

I. Introduction

PID control scheme has become the mostly used controller in many industries, particularly the high-tech industry [1] due to robustness and ease of use through the loop-shaping method. However, being inherently linear, it suffers from fundamental limitations, which are the waterbed effect and Bode's gain phase relation [2] [3]. One novel approach called reset control has gained increasing attention due to its compatibility with frequency domain techniques for design and analysis, which are popular within industry.

In reset control, the states of the base linear system of the controller are reset when a predefined condition is satisfied. The first reset element introduced was a Clegg Integrator (CI) in 1958 [4], which is an integrator whose state is reset to zero when the input is zero. Using a pseudo-linear frequency response description of nonlinear controllers called Describing Function (DF) [5], the frequency response of the CI is obtained, which reveals a similar gain performance as the linear integrator but with only -38° phase lag. This is advantageous since this violates Bode's gain phase relationship, allowing improved performance without sacrificing stability. The idea of reset has also been extended to more sophisticated elements such as First Order Reset Element (FORE) [6] [7] and Second order Reset Element (SORE) [8]. These elements have been successfully applied to satisfy various objectives such as phase lag reduction [9], broadband phase compensation [10], improving servomotor performance [11], and improvement of mid frequency disturbance rejection [12].

Frequency response of reset controllers can be approximated using the aforementioned DF method [5]. However, since it is an approximation, the advantages described previously is not always seen in practice. This is because of non-linearity in the form of higher order harmonics in the output of reset controllers are not considered by the DF method. These higher order harmonics are analyzed in open loop through HOSIDF method [13] and recently in closed loop [14]. There exists a need to reduce the higher order harmonics such that the output is dominated by the first harmonic, which makes the benefit of reset control predicted by the DF consistently realizable. This paper presents a novel augmented analogue for the reset integrator with the aim of obtaining the same first harmonic behavior while reducing the higher order harmonics.

The paper is structured as follows. Section II of this paper will introduce reset control. Section III examines the fractional order augmented state reset integrator and the benefits it possesses over the traditional reset integrator. Section IV gives an illustrative example of benefits of using the augmented state reset integrator through simulation and experimental validation of disturbance rejection on a precision positioning system. Conclusions and possible future work are outlined in section V.

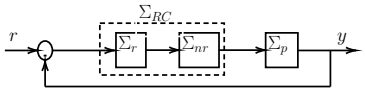

Fig. 1: Block diagram of a reset controller RC with a plant P

II. Reset Control

A. Definition

A single-input single-output (SISO) reset controller (denoted Σ_{RC}) is defined as

$$\begin{cases} \dot{x}(t) = A_r x(t) + B_r e(t) & \text{if } e(t) \neq 0 \\ x(t^+) = A_\rho x(t) & \text{if } e(t) = 0 \\ u(t) = C_r x(t) + D_r e(t) \end{cases} \quad (1)$$

Here $x(t)$ are the states, and A_r, B_r, C_r and D_r are the matrices corresponding to state-space representation of the base linear system of the controller. $e(t)$ and $u(t)$ are the input and output of the controller respectively. A_ρ is a diagonal matrix that dictates the after-reset values of the states.

Theorem 1: [15] The reset controller defined by equation (1) with a sinusoidal input has a $\frac{2\pi}{\omega}$ periodic solution that is globally asymptotically stable for all $\omega > 0$ if and only if

$$|\lambda(A_\rho e^{\Delta})| < 1 \quad (2)$$

where $\Delta = \frac{\pi}{\omega} A_r$. This theorem consequently constraints each member of the diagonal of A_ρ to be between -1 and 1.

B. Reset Systems Stability

Figure 1 shows a reset controller Σ_{RC} with a plant Σ_P. As shown in the figure, the reset controller can be decomposed into a reset part Σ_r and a non reset part Σ_{nr}. Let n_r and n_{nr} therefore denote the number of reset and non reset states of Σ_{RC} respectively.

Theorem 2: [16] The reset control system depicted in figure (1) is quadratically stable if and only if the H_β condition holds, i.e. there exists a $\beta \in \mathbb{R}^{n_r}$ and a positive definite matrix $P_r \in \mathbb{R}^{n_r \times n_r}$ such that the transfer function

$$Z_\beta(s) := \begin{bmatrix} \beta C_p & 0_{n_r \times n_{nr}} & P_r \end{bmatrix} (sI - A_{cl})^{-1} \begin{bmatrix} 0_{n_p} \\ 0_{n_{nr} \times n_r} \\ I_{n_r} \end{bmatrix} \quad (3)$$

is strictly positive real. Here A_{cl} is the closed loop A matrix of Figure 1 defined as:

$$A_{cl} = \begin{bmatrix} A_p & B_p C_{RC} \\ -B_{RC} C_p & A_{RC} \end{bmatrix}$$

in which (A_p, B_p, C_p) are the state space matrices of Σ_p, and (A_{RC}, B_{RC}, C_{RC}) are the state space matrices of Σ_{RC}.

C. Describing function

Describing Function (DF) is a pseudo-linear approximation of the frequency response of reset controllers. Since it only considers the first harmonic of the output, expected experimental results based on loop shaping are not seen [10]. Nuij et. al. [5] developed the concept of higher order sinusoidal input describing function (HOSIDF), which is further developed by Kars [13] specifically for reset elements. The HOSIDF formula for reset elements is as shown:

$$H_n(j\omega) = \begin{cases} C_r (jwI - A_r)^{-1} (I + j\theta_D(\omega)) B_r + D_r & \text{for } n = 1 \\ C_r (j\omega n I - A_r)^{-1} j\theta_D(\omega) B_r & \text{for odd } n \geq 2 \\ 0 \quad \text{for even } n \geq 2 \end{cases} \quad (4)$$

where

$$\begin{aligned} \theta_D(\omega) &\triangleq -\frac{2\omega^2}{\pi} \Delta(\omega) \left[\Gamma_D(\omega) - \Lambda^{-1}(\omega)\right] \\ \Delta(\omega) &\triangleq I + e^{\frac{\pi}{\omega} A_r} \\ \Lambda(\omega) &\triangleq \omega^2 I + A_r^2 \\ \Gamma_D(\omega) &\triangleq \Delta_D^{-1} A_\rho \Delta \Lambda^{-1} \\ \Delta_D(\omega) &\triangleq I + A_\rho e^{\frac{\pi}{\omega} A_r} \end{aligned}$$

Here, n indicates the number of harmonic. The DF is therefore a special case of HOSIDF with $n = 1$.

III. Augmented Fractional-order State Reset Integrator

Fractional calculus generalizes integration and differentiation to real or complex number powers. There exist multiple accepted definitions of fractional differentiation. The notation $D^k x(t)$, $k \in [0, 1]$ in this paper will refer to the Caputo definition defined in [17].

A. Augmented system of fractional order reset integrator

A fractional order reset integrator is defined as:

$$\begin{aligned} D^k x(t) &= e(t) \\ x(t^+) &= \gamma x(t) \\ u(t) &= x(t) \end{aligned} \quad (5)$$

where $k \in [0, 1]$.

The fractional order integrator is implemented through the CRONE approximation [18] with its poles being reset, defined by:

$$s^{\gamma} \approx P \prod_{m=1}^{N} \frac{1+\frac{s}{\omega_{z,m}}}{1+\frac{s}{\omega_{p,m}}}^{A_\rho} \tag{6}$$

with

$$\omega_{z,m} = \omega_l \left(\frac{\omega_n}{\omega_l}\right)^{\frac{2m-1-\alpha}{2N}}$$

$$\omega_{p,m} = \omega_1 \left(\frac{w_h}{w_l}\right)^{\frac{2m-1+\alpha}{2N}}$$

where $\alpha \in (0,1)$, N is the number of real stable poles and real minimum phase zeros, $[\omega_l, \omega_h]$ is the frequency range where the approximation is valid, and P is a parameter to tune the gain of the approximation. A_ρ is a reset matrix that corresponds to the reset of the fractional order integrator γ.

Remark 1: A_ρ is dependent on the chosen state space representation of the approximation. With an observable canonical form, only the last state of the approximation directly influences the output, and thus the corresponding reset matrix becomes

$$A_\rho = \begin{bmatrix} \boldsymbol{I} & \boldsymbol{0} \\ \boldsymbol{0} & \gamma \end{bmatrix} \tag{7}$$

However, with controllable canonical form, all states influence the output, and thus the reset matrix is:

$$A_\rho = \begin{bmatrix} \gamma_1 & & \\ & \ddots & \\ & & \gamma_N \end{bmatrix} \tag{8}$$

B. Augmented system of integer order reset integrator

The integer-order state reset integrator is obtained by setting $k = 1$ in 5. The augmented fractional order form of this case is given by:

$$\begin{aligned} D^q \chi(t) &= \mathbf{A}\mathcal{X}(t) + \mathbf{B}e(t) \\ \mathcal{X}(t^+) &= \mathbf{A}_\rho \mathcal{X}(t) \\ u(t) &= \mathbf{C}\mathcal{X}(t) \end{aligned} \tag{9}$$

where,

$$\mathbf{A} = \begin{bmatrix} \boldsymbol{0} & \boldsymbol{I} \\ \boldsymbol{0} & \boldsymbol{0} \end{bmatrix}, \quad \mathbf{A}_\rho = \begin{bmatrix} \gamma & \boldsymbol{0} \\ \boldsymbol{0} & \boldsymbol{I} \end{bmatrix}$$

$$\mathbf{B} = \begin{bmatrix} 0 \\ \vdots \\ 1 \end{bmatrix}, \mathbf{C} = \begin{bmatrix} 1 & \dots & 0 \end{bmatrix}$$

Here $\mathcal{X} = [x\, x_{q,1}\, x_{q,2} \dots x_{q,p-1}]^T$ is a vector of the augmented states and $p = \frac{1}{q}$, where $p \in \mathbb{Z}^+$.

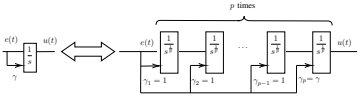

Fig. 2: Illustration of equivalence between cascade of fractional order integrators and an integer reset integrator. The arrows indicate that the reset of each element is with respect to the input to the cascade i.e. $e(t)$

C. Equivalence of cascaded fractional order reset integrators with augmented integer order reset integrator

Remark 2: Consider figure 2. The cascade of p fractional order reset integrators in series is equivalent to the augmented form of an integer reset integrator with $q = \frac{1}{p}$.

Proof: Let k be the k^{th} fractional order reset integrator, with $1 \leq k \leq p$. The state space representation becomes:

$$\begin{aligned} D^{1/p} x_k(t) &= e_k(t) \\ x_k(t^+) &= \gamma_k x_k(t) \\ u_k(t) &= x_k(t) \end{aligned} \tag{10}$$

With $e_1(t) = e(t)$, $e_k = u_{k-1}$ and $u_p(t) = u(t)$, the combined state space of the cascade is simplified to:

$$\begin{aligned} D^{1/p} \begin{bmatrix} x_1(t) \\ \vdots \\ x_p(t) \end{bmatrix} &= \begin{bmatrix} \boldsymbol{0} & \boldsymbol{0} \\ \boldsymbol{I} & \boldsymbol{0} \end{bmatrix} \begin{bmatrix} x_1(t) \\ \vdots \\ x_p(t) \end{bmatrix} + \begin{bmatrix} 1 \\ \vdots \\ 0 \end{bmatrix} e(t) \\ u(t) &= \begin{bmatrix} 0 & \dots & 1 \end{bmatrix} \begin{bmatrix} x_1(t) \\ \vdots \\ x_p(t) \end{bmatrix} \end{aligned} \tag{11}$$

where $x_1 = D^{1/p} x_2$, $x_2 = D^{1/p} x_3$, $\dots$, $x_{p-1} = D^{1/p} x_p$.

Considering remark 1, since the output of the cascade is only influenced by the state $x_p(t)$, the appropriate reset matrix for the cascade is:

$$A_\rho^{cascade} = \begin{bmatrix} \boldsymbol{I} & \boldsymbol{0} \\ \boldsymbol{0} & \gamma_p \end{bmatrix} \tag{12}$$

Reverse the ordering of the state vector above such that x_p becomes in the first entry. With $q = 1/p$ and $\gamma_p = \gamma$, this results in state space that is equal to (9). Therefore equivalence is proven and the cascade is a valid replacement of the integer-order reset integrator.

Remark 3: [19] Let the reset control system Σ_{RC} in figure 1 be composed of firstly a reset element Σ_r

followed by a lag element Σ_{nr}. The higher order harmonics gain of Σ_{RC} is smaller than Σ_r if Σ_{nr} is a linear lag element:

$$|H_n(j\omega)|_R < |H_n(j\omega)|_{\Sigma_r}, \quad \text{odd}\, n > 1 \tag{13}$$

Remark 4: Consider a reset integrator with reset value γ. With $-1 < \gamma \leq 1$, the following relation holds:

$$-90^\circ \leq \angle H_1(j\omega) < 0^\circ \tag{14}$$

where -90° corresponds to $\gamma = 1$ (linear integrator) and 0° corresponds to $\gamma = -1$.

Remark 4 also holds for the fractional order reset integrator of 5, with the lower limit changed to $-90^\circ k$.

Based on remark 2, (11) is the analogue to the reset integrator if $\gamma_p = \gamma$ and $\gamma_k = 1$, $\forall\, k \leq p-1$. It therefore follows that not only the first but also higher order harmonics are similar. However, it is desired to reduce the higher order harmonics while maintaining the first order harmonic behavior. Considering remark 3 and 4, this could be achieved through a combination of $\gamma_1, \ldots, \gamma_p$ that does not necessarily satisfy the aforementioned restriction on γ_p and γ_k. Therefore, the goal of this paper is to design $\gamma_1, ..., \gamma_p$ such that the first harmonic is the same as the reset integrator while simultaneously possessing lower higher order harmonic gain.

This goal is casted in an optimization problem as shown:

$$\min_{\gamma_{Aug}=[\gamma_1,\gamma_2,\ldots,\gamma_p]} |H_n(\gamma_{Aug}, j\omega)|_{Aug} \tag{15}$$
$$\forall\, n > 1 \,\text{odd}\, n,\ \forall \omega \in [\omega_l, \omega_h]$$
$$\text{subject to}$$
$$|H_1(\gamma_{Aug}, j\omega)|_{Aug} = |H_1(\gamma, j\omega)|_{\text{Reset Integrator}}$$
$$\angle H_1(\gamma_{Aug}, j\omega)_{Aug} = \angle H_1(\gamma, j\omega)_{\text{Reset Integrator}}$$

where Aug refers to the fractional order analogue of the reset integrator. For simplicity, the optimization will be run for $p = 2$, 3 and 4 and the reductions in higher order harmonics magnitude will be compared. In addition, non-zero values of γ will also be considered.

D. Results

Table I shows the third order harmonic gain for different reset values of the reset integrator and its respective augmented fractional order analogue for $p = 2$, 3 and 4. Instead of the different reset values, by utilizing remark 4, the horizontal axis of this figure alternatively shows the phase lag that the reset integrator provides. Table I shows the reset values of the augmented states for each value of p and the optimal reset values. Some observation:

- For all p and phase lag values, the integrator nearing the end of the cascade is more linear than those nearing the start, which satisfies remark 2.
- As the required phase lag decreases, the reset value of the integrators near the end of the cascade is not fully linear. Considering remark 3, this indicates that the starting integrators cannot provide all the required phase lag reduction, and thus the integrators near the end provide some support in this regard.
- There is more reduction of the third order harmonic for larger phase lag. Thus there exists a tradeoff between obtaining larger reduced phase lag advantage and the corresponding third harmonic gain reduction.
- The further reduction in third harmonic gain by going from $p = 2$ to $p = 3$ or $p = 4$ is insignificant compared to reduction from the original reset integrator to $p = 2$ case. Therefore it is recommended to use $p = 2$ in implementation.

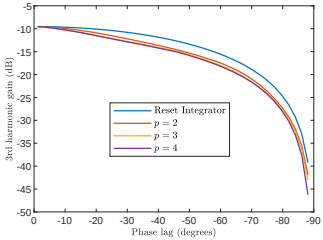

Fig. 3: 3rd order harmonic gain at $\omega = 100rad/s$ of various p values, for different provided phase lag

E. Non-Zero Higher Order Harmonic Phase

In this subsection it will be shown how the non-zero higher order harmonics phase of the augmented fractional-order state analogue could be of benefit.

The time domain output of a reset element given a sinusoidal input $\sin(\omega t)$ is:

$$u(t) = \sum_{m=1}^{\infty} A_m sin(\omega t + \phi_m), \,\text{odd}\, m \geq 1 \tag{16}$$

The above emphasizes that not only the gain but the higher order harmonics phase also influence the output of the reset element.

To investigate this, the RMS difference between the time domain response of the reset integrators and the ideal response is computed, where the ideal response is

Reset Integrator		
γ	Equivalent Phase Lag (°)	3rd harmonic gain (dB)
-0.8	-5.00	-9.57
-0.4	-18.60	-10.00
0	-38.15	-11.63
0.4	-61.38	-15.94
0.8	-81.95	-26.62

Augmented analogue, $p = 2$				
γ	Equivalent Phase Lag (°)	γ_2	γ_1	3rd harmonic gain (dB)
-0.8	-5.00	-0.98	-0.74	-9.71
-0.4	-18.60	-0.98	-0.11	-10.83
0	-38.15	-0.97	0.66	-13.56
0.4	-61.38	-0.38	1.00	-18.44
0.8	-81.95	0.59	1.00	-29.32

Augmented analogue, $p = 3$					
γ	Equivalent Phase Lag (°)	γ_3	γ_2	γ_1	3rd harmonic gain (dB)
-0.8	-5.00	-0.97	-0.97	-0.66	-9.80
-0.4	-18.60	-0.95	-0.95	0.27	-11.25
0	-38.15	-0.75	-0.71	1.00	-13.72
0.4	-61.38	-0.6	0.48	1.00	-18.55
0.8	-81.95	0.35	1.00	1.00	-29.68

Augmented analogue, $p = 4$						
γ	Equivalent Phase Lag (°)	γ_4	γ_3	γ_2	γ_1	3rd harmonic gain (dB)
-0.8	-5.00	-0.94	-0.92	-0.87	-0.64	-9.81
-0.4	-18.60	-0.95	-0.92	-0.87	0.53	-11.34
0	-38.15	-0.97	-0.82	0.18	1.00	-13.73
0.4	-61.38	-0.43	-0.23	1.00	1.00	-18.60
0.8	-81.95	0.16	1.00	1.00	1.00	-30.20

TABLE I: Reset values and 3rd harmonic gain at $\omega = 100rad/s$ of each augmented state for various p values, the subscripts for the various γ correspond to figure 2

the response of the reset integrator with all the higher order harmonic gains eliminated. Figure 4 shows this RMS difference for different values of the higher order harmonics phase. At -48.5° there exists a minimum of the RMS difference. The reset integrator however, has zero higher order harmonics phase and so this minimum cannot be achieved.

In contrast, the augmented fractional-order state analogue has a negative higher order harmonics phase. For instance the third harmonic phase is shown in figure 5 for $p = 2$. Therefore in addition to lower higher order harmonics gain, the augmented fractional-order state analogue also possess a beneficial higher order harmonics phase behavior.

IV. Illustrative Example

For validation in performance improvement of a system that utilizes the augmented fractional state analogue, four controllers are designed and studied in simulation and in practice. This section compares results of disturbance rejection performance between a parallel PID (termed PI+D) and three other parallel PID respectively in series with a linear integrator, Clegg Integrator and augmented fractional state analogue of the Clegg Integrator with $p = 2$.

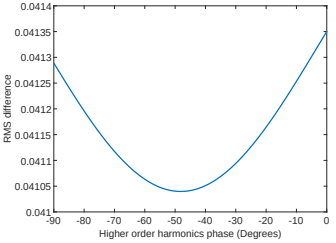

Fig. 4: Higher order harmonics phase vs. RMS Error of reset integrator with $\gamma = 0$

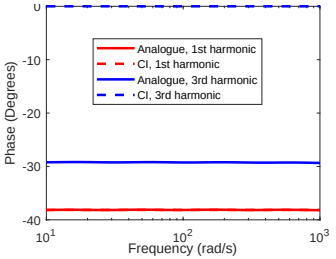

Fig. 5: Phase plot of 1st and 3rd harmonic of the CI vs. augmented fractional-order analogue

1) Plant

The plant use for this validation is a two flexure-guided fine stage guided by a Lorentz actuator as shown in figure 12, with figure 6 describing its identified frequency response and additionally a fitted second order transfer function. The position of the plant is sensed using a laser interferometer with 10nm resolution, with the sampling period of the plant at 100μs.

The fitted transfer function is:

$$G(s) = \frac{3.038e4}{s^2 + 0.7413s + 243.3} \tag{17}$$

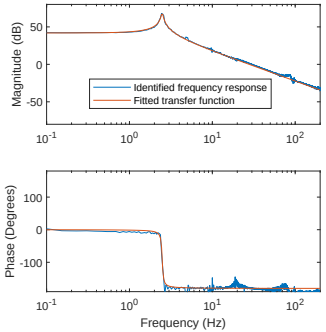

Fig. 6: Identified frequency response of the fine stage

2) Control Strategy

Four sets of controllers are designed with a bandwidth of 100 Hz: a parallel PID controller (PI+D), a parallel PID with an extra tamed integrator ((PI+D)PI), a parallel PID with an extra tamed Clegg Integrator ((PCI+D)PI), and a parallel PID with an extra tamed augmented fractional order analogue of Clegg Integrator ((PCI$_{aug}$+D)PI). Figure 7 depicts the details of these controllers. As shown in figure 8, the (PI+D)PI controller was able to outperform PI+D in terms of gain performance, however with the tradeoff of phase margin reduction. Considering the reduced phase lag advantage of a Clegg Integrator, it is surmised that the (PCI+D)PI controller could be tuned to have less phase margin reduction while still maintaining the gain behavior of (PI+D)PI, which is indeed the case as shown in yellow and blue in 8. To verify this result, figure 9 shows simulation result of disturbance rejection performance to 1 Hz disturbance input. Contrary to expected performance from 8, the simulation plot shows (PCI+D)PI performing far worse compared to (PI+D)PI; this is because figure 8 shows only the first order harmonic.

To reduce the effects of the higher order harmonics, the augmented fractional-order analogue replaces the Clegg Integrator (giving the controller (PCI$_{aug}$I+D)PI), with tuned open loop performance shown in purple in figure 8. The simulation result is also shown in purple in figure 9. From these figures it is observed that the phase margin of (PCI+D)PI is still maintained, while

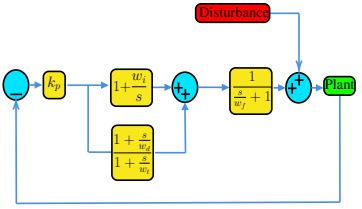

(a) PI+D

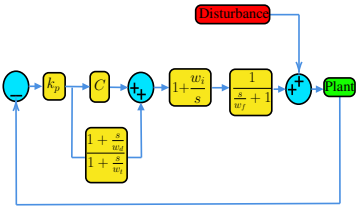

$$C = 1+\frac{w_i}{s} \quad \Rightarrow \quad (PI+D)PI$$
$$C = 1+\frac{w_i}{s} \quad \gamma = 0 \quad \Rightarrow \quad (PCI+D)PI$$
$$C = 1+\frac{w_i}{s} \quad {}^{PCI_{Aug}} = [-0.97, 0.66] \quad \Rightarrow \quad (PCI_{Aug}+D)PI$$

(b) Control schemes used for the adapted PI+D controllers

Fig. 7: Control scheme definitions for validation. Disturbance refers to an applied sinusoidal disturbance input

the jump size in figure 9 reduced in magnitude, making the maximum amplitude of the response now closer to (PI+D)PI.

To see whether this improvement exists over a range of frequencies, a process sensitivity function is constructed. To capture the higher order harmonics in the process sensitivity function plot for the controllers with reset elements, a new process sensitivity function is defined as:

$$S(\omega) = \frac{max(|y(t)|)}{|D|} \quad \text{for } t \geq t_{ss} \qquad (18)$$

where t_{ss} is the time it takes for the response to become

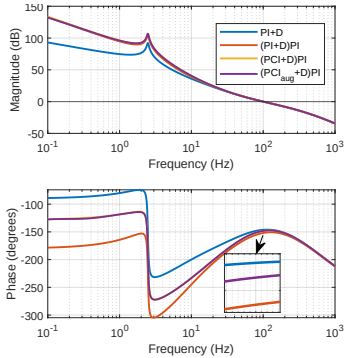

Fig. 8: Open loop frequency response of control scheme in figure 7. The gain and phase response of (PCI+D)PI (yellow) is on top of (PCI$_{aug}$+D)PI (purple)

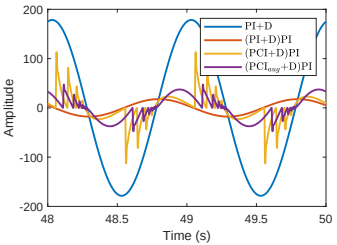

Fig. 9: Response of control scheme in figure 7 to a 1 Hz disturbance, using each of the four different extra controllers

steady state and periodic, $y(t)$ is the output and D is the amplitude of the sinusoidal disturbance input. This function is found by simulating the closed loop system with a disturbance input for increasing, closely spaced ω. The plot is shown in figure 10. Here it is seen that compared to (PCI+D)PI, (PCI$_{aug}$I+D)PI's performance is closer to (PI+D)PI up to approximately 4 Hz, from which the performance of all the reset controllers are now able to match (PI+D)PI.

It is also noted that the higher stability level of the (PCI+D)PI and the (PCI$_{aug}$I+D)PI compared to (PI+D)PI and PI+D, which was implied by their higher phase margin from figure 8, was also taken by utilizing the

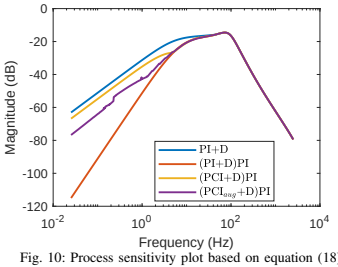

Fig. 10: Process sensitivity plot based on equation (18)

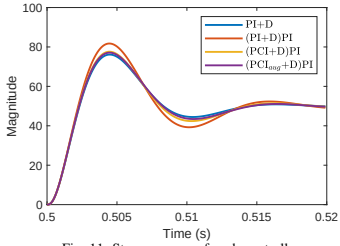

Fig. 11: Step response of each controller

Descibing Function. This therefore means that the true stability level may not be the same as what the DF predicted in this figure. To check that the higher stability level indeed truly exist, the peak of the step response is examined, with a lower overshoot indicating higher stability. This is shown in figure 11. Here it is observed that both (PCI+D)PI and (PCI$_{aug}$I+D)PI have a lower overshoot, which indicates a higher stability level has indeed been achieved.

3) Stability Check Using H_β condition

To further confirm the stability of the fractional order analogue, the H_β condition described in section II is also applied on the control scheme 7. Solving the condition using a YALMIP Sedumi solver [20], a positive definite matrix P_r was indeed found, further confirming that the fractional order analogue is indeed stable.

Dist.	$max(\lvert y(t)\rvert)(10\,nm)$			
(Hz)	PI+D	(PI+D)PI	(PCI+D)PI	(PCI$_{aug}$+D)PI
0.1	21	3	14	13
0.2	32	3	25	20
0.3	56	4	37	35
0.4	74	5	49	40
0.5	93	7	61	46
0.6	110	8	72	62
0.7	127	12	84	69
0.8	146	14	96	78
0.9	163	13	107	85
1	178	19	116	89
2	341	68	206	146
3	476	137	263	250
4	582	216	296	290
Step input	$max(\lvert y(t)\rvert)(10\,nm)$			
1000	1492	1611	1515	1517

TABLE II: Experiment results. Disturbance input amplitude is 6528 ($10nm$) and step input size is 1000 ($10nm$)

V. Experiment results

1) Results

To validate the closed loop simulation results, an experiment is conducted. Disturbances of selected frequencies are chosen, and the amplitude of the plant response are recorded. To check the stability level, a step input is also applied.

Table II shows the maximum response of the plant controlled by each of the four different controllers. It is seen that the trend in the simulation result is confirmed, with the (PCI$_{aug}$+D)PI outperforms (PCI+D)PI and PI+D in the frequency region predicted by the simulation in figure 10. In addition, the step response of the (PCI+D)PI and the (PCI$_{aug}$+D)PI also exhibit a similar overshoot value, indicating that the increased stability level predicted by simulation is also seen in experiment.

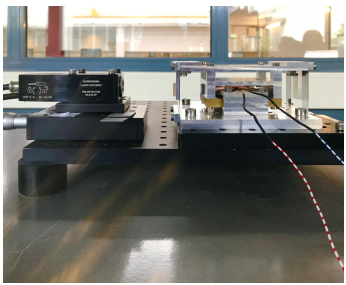

Fig. 12: Fine stage used in experiment

VI. Conclusion

Reset controller is a subset of nonlinear controllers that overcomes the fundamental limitations of linear controller, while still retaining the advantage of linear controllers in that the loop shaping method is applicable through the Describing Function method. However, the Describing Function does not take into account higher order harmonics, which makes the actual output of the controller sometimes deviate from that predicted using the Describing Function. It is then desired to minimize the role of these higher order harmonics on influencing the output.

Augmented fractional-order reset integrator analogue is a promising method in achieving this goal. By resetting the fractional states of the reset integrator to a determined optimal values, it has been shown that there is a higher order harmonics reduction that may not seem huge in open-loop, however results in a significant closed loop performance improvement. A recommendation was then made as to the reset values of the fractional states required for a particular tolerable phase lag. Furthermore, the non-zero higher order harmonics phase that the augmented fractional-order reset integrator analogue possess was shown to be promising in further improving the output of the reset integrator.

For future work, it is recommended to develop a tuning rule for the state space representation of the augmented fractional-order analogue such that the higher order harmonics phase can be manipulated to obtain the optimal reduction in the RMS difference discussed in section 4.4, while still maintaining reduced higher order harmonic gains. A final recommendation is to also investigate resetting the fractional elements with respect to their own respective inputs as opposed to the error; there may be aspects of the intermediate signals that could bring about more higher order harmonic reductions.

References

[1] Tariq Samad et al. “IFAC Industry Committee Update, Initiative to Increase Industrial Participation in the Control Community”. In: *Newsletters April 2019*. IFAC, 2019.

[2] Robert Munnig Schmidt, Georg Schitter, and Jan van Eijk. *The design of high performance mechatronics*. 2014. ISBN: 9781607508250.

[3] Antonio Barreiro and Alfonso Bãnos. “Reset control systems”. In: *RIAI - Revista Iberoamericana de Automatica e Informatica Industrial*. 2012. Chap. 1, pp. 11–17. DOI: 10.1016/j.riai.2012.09.007.

[4] J. C. Clegg. “A nonlinear integrator for servomechanisms”. In: *Transactions of the American*

Institute of Electrical Engineers, Part II: Applications and Industry (2013). ISSN: 0097-2185. DOI: 10.1109/tai.1958.6367399.

[5] P. W.J.M. Nuij, O. H. Bosgra, and M. Steinbuch. "Higher-order sinusoidal input describing functions for the analysis of non-linear systems with harmonic responses". In: *Mechanical Systems and Signal Processing* 20.8 (2006), pp. 1883–1904. ISSN: 08883270. DOI: 10.1016/j.ymssp.2005.04.006.

[6] Isaac Horowitz and Patrick Rosenbaum. "Nonlinear design for cost of feedback reduction in systems with large parameter uncertainty". In: *International Journal of Control* 21.6 (1975), pp. 977–1001. ISSN: 13665820. DOI: 10.1080/00207177508922051.

[7] Luca Zaccarian, Dragan Nešić, and Andrew R. Teel. "First order reset elements and the Clegg integrator revisited". In: *Proceedings of the American Control Conference*. 2005. DOI: 10.1109/acc.2005.1470016.

[8] Leroy Hazeleger, Marcel Heertjes, and Henk Nijmeijer. "Second-order reset elements for stage control design". In: *Proceedings of the American Control Conference*. 2016, pp. 2643–2648. ISBN: 9781467386821. DOI: 10.1109/ACC.2016.7525315.

[9] M. F. Heertjes et al. "Design of a variable gain integrator with reset". In: *Proceedings of the American Control Conference*. 2015. ISBN: 9781479986842. DOI: 10.1109/ACC.2015.7171052.

[10] Niranjan Saikumar, Rahul Kumar Sinha, and S. Hassan Hosseinnia. "'Constant in Gain Lead in Phase' Element-Application in Precision Motion Control". In: *IEEE/ASME Transactions on Mechatronics* (2019). ISSN: 1941014X. DOI: 10.1109/TMECH.2019.2909082. arXiv: 1805.12406.

[11] S. Hassan HosseinNia, Inés Tejado, and Blas M. Vinagre. "Fractional-order reset control: Application to a servomotor". In: *Mechatronics* 23.7 (2013), pp. 781–788. ISSN: 09574158. DOI: 10.1016/j.mechatronics.2013.03.005.

[12] Ying Li, Guoxiao Guo, and Youyi Wang. "Nonlinear mid-frequency disturbance compensation in hard disk drives". In: *IFAC Proceedings Volumes (IFAC-PapersOnline)*. 2005. ISBN: 008045108X.

[13] Kars Heinen. "Frequency analysis of reset systems containing a Clegg integrator". 2018. URL: https://repository.tudelft.nl/islandora/object/uuid{\%}3Accc37af2-fcbc-46ec-9297-afdc5c1ea4b5.

[14] Ali Dastjerdi et al. "Closed-loop frequency analyses of reset systems". 2020. URL: https://arxiv.org/abs/2001.10487.

[15] Yuqian Guo, Yuoyi Wang, and Lihua Xie. "Frequency-domain properties of reset systems with application in hard-disk-drive systems". In: *IEEE Transactions on Control Systems Technology* 17.6 (2009), pp. 1446–1453. ISSN: 10636536. DOI: 10.1109/TCST.2008.2009066.

[16] Orhan Beker et al. "Fundamental properties of reset control systems". In: *Automatica* 40.6 (2004), pp. 905–915. ISSN: 00051098. DOI: 10.1016/j.automatica.2004.01.004.

[17] Michele Caputo. "Linear Models of Dissipation whose Q is almost Frequency Independent-II". In: *Geophysical Journal of the Royal Astronomical Society* (1967). ISSN: 1365246X. DOI: 10.1111/j.1365-246X.1967.tb02303.x.

[18] A. Oustaloup and M. Bansard. "First generation CRONE control". In: *Proceedings of the IEEE International Conference on Systems, Man and Cybernetics*. 1993. ISBN: 0780309111. DOI: 10.1109/icsmc.1993.384861.

[19] Chengwei Cai et al. "The Optimal Sequence for Reset Controllers". 2019. URL: https://www.semanticscholar.org/paper/The-Optimal-Sequence-for-Reset-Controllers-by-Cai-Dastjerdi/ea0ac3b0d2868255e2107699a62b56cfe85b0d58.

[20] Johan Löfberg. "YALMIP: A toolbox for modeling and optimization in MATLAB". In: *Proceedings of the IEEE International Symposium on Computer-Aided Control System Design*. 2004, pp. 284–289. DOI: 10.1109/cacsd.2004.1393890.

[21] Samir Mittal and Chia Hsiang Menq. "Precision motion control of a magnetic suspension actuator using a robust nonlinear compensation scheme". In: *IEEE/ASME Transactions on Mechatronics* (1997). ISSN: 10834435. DOI: 10.1109/3516.653051.

[22] Ralph J. Kochenburger. "A Frequency Response Method for Analyzing and Synthesizing Contactor Servomechanisms". In: *Transactions of the American Institute of Electrical Engineers* 69.1 (1950), pp. 270–284. ISSN: 00963860. DOI: 10.1109/T-AIEE.1950.5060149.

[23] N. M Krylov and N. Bogoliubov. *Introduction to Nonlinear Mechanics*. 1943. ISBN: 0691079854.

[24] S. Hassan HosseinNia, Inés Tejado, and Blas M. Vinagre. "Fractional-order reset control: Application to a servomotor". In: *Mechatronics* (2013). ISSN: 09574158. DOI: 10.1016/j.mechatronics.2013.03.005.

[25] K. J. Åström and T. Hägglund. “The future of PID control”. In: *Control Engineering Practice* 9.11 (2001), pp. 1163–1175. ISSN: 09670661. DOI: 10.1016/S0967-0661(01)00062-4.

[26] Shih Kang Kuo, Ximin Shan, and Chia Hsiang Menq. “Large travel ultra precision x - y θ motion control of a magnetic-suspension stage”. In: *IEEE/ASME Transactions on Mechatronics* 2.4 (2003), pp. 268–280. ISSN: 10834435. DOI: 10.1109/TMECH.2003.816825.

[27] Duarte Valério et al. “Reset control approximates complex order transfer functions”. In: *Nonlinear Dynamics* (2019), pp. 3–4. ISSN: 1573269X. DOI: 10.1007/s11071-019-05130-2.

5

CONCLUSION

5.1. FINDINGS

The research goal of this thesis is:

Find the analogue of the reset integrator that has reduced higher order harmonics while maintaining the first order harmonic performance of the reset Integrator, and confirm that this reduction translate to improved performance in closed loop.

Based on an understanding of fractional elements at different reset values, optimization and time domain simulations, the results obtained are:

- There indeed exist reduction of higher order harmonics through the use of the augmented analogue, with the corresponding reset values of the analogue conforming to the filtering of higher order harmonics theory alluded to by Cai [9].
- Breaking the analogue from two elements to further smaller elements do produce further reduction in higher order harmonics, however the reduction is insignificant and therefore is not recommended to be used.
- The non-zero higher order harmonics of the analogue was manipulated; this manipulation do indeed produce further improvement in the output of the element. At the value of $-52°$, the RMS error of the output of the analogue is minimum, with a smaller value than the RMS error of CI.
- The disturbance rejection performance of a controller incorporating the CI analogue ($PCI_{aug}+D)PI$) instead of a CI (($PCI+D)PI$)) is investigated to check whether the benefits of reduced higher order harmonics translate to a better closed loop performance. Due to higher order harmonics, $(PCI+D)PI$ is unable to approach the disturbance rejection performance of a $(PI+D)PI$ controller despite being tuned in open loop to do so. Replacing the CI with its augmented analogue, $(PCI_{aug}+D)PI$ is able to approach the performance of $(PI+D)PI$ better compared to $(PCI+D)PI$, by improved disturbance rejection performance over frequency ranges where disturbances are relevant.

Appendix A attempts an analysis as to why using more elements in the integrator do not produce further significant reduction in higher order harmonics. In Appendix B, an investigation is done on the effects of using a lead element in the analogue in order to allow integrating behavior even outside the fractional order element's approximation frequency range. With the plant under investigation having a resonance peak, Appendix C verifies that usage of a parallel PID indeed produces a lower higher order harmonics contribution to the closed loop scheme, and also investigates adding a notch filter and seeing the effects in the disturbance rejection investigation. Although adding the notch filter further improves the reliability of the Describing Function of the reset controllers by reducing the higher harmonic peak at the resonant frequency of the plant, the disturbance rejection performance at the resonant frequency of the plant is highly worsened.

Appendix D investigates performance improvement in other areas than disturbance rejection; this is not included in the above paper because experimental validation was not conducted on these areas. Appendix E describes the system used for experimental validation in the paper, and Appendix F checks the stability of the analogue using H_β condition.

5.2. RECOMMENDATIONS

For further study, the following points are recommended:

- This thesis has shown that manipulation of the non-zero phase of higher order harmonics of the analogue produce a better time domain output compared to CI. A further study could be to find a tuning rule that finds the optimal state space representation of the analogue, such that the higher order harmonics reduction is maintained while simultaneously producing higher order harmonics phase that further reduces the RMS difference between time domain output of analogue and the first harmonic of CI.
- A different experiment set up could be used to verify that the superiority of the analogue is not unique to the fine stage used in this thesis.
- In this thesis, the reset of each of the elements that make up the analogue is based on the zero crossing of the input to the first element of the analogue. A further study could investigate looking at resetting the elements based on the zero crossing of the inputs to each of the elements; whether doing so could produce further significant higher order harmonics reduction.
- The analogue was found only for a reset integrator. Further investigation could be to find the analogue for more complicated elements such as FORE or SORE.

A

THIRD HARMONIC REDUCTION FOR MORE ELEMENTS

In the paper, further reduction of third harmonic gain by using more elements was found to not be significant. This appendix attempts to explain the reason.

First it is investigated as to why using more elements could contribute to lower higher order harmonic. Figure A.1a shows the first order harmonic phase as a function of contributed phase lag for $\frac{1}{s^{1/2}}$ and a smaller element $\frac{1}{s^{1/3}}$; here smaller is in the sense of the power of the fractional integrator. At a very low reset value ($\gamma = -0.8$), $\frac{1}{s^{0.33}}$ is still able to obtain the same phase lag as $\frac{1}{s^{0.5}}$. This implies that with two of $\frac{1}{s^{0.33}}$, each of $\frac{1}{s^{0.33}}$ can have more moderate reset values while the combination still providing the required phase lag advantage, making the higher order harmonics produced by the combination not as large as $\frac{1}{s^{0.5}}$ due to the less aggressive reset of each of them.

From looking at the reset values of the analogue for reset integrator with $\gamma = 0$, the integrators that provide the phase lag advantage case for $p = 3$ indeed has more moderate reset values compared to $p = 2$, which contribute to less higher order harmonic contribution.

However, looking at figure A.1b, the integrator that filters higher order harmonics for $p = 3$ has a less steep slope, which makes the filtering behaviour less effective compared to $p = 2$. Therefore, it is concluded that exists a tradeoff by using more elements; there is reduced contribution of higher order harmonics, however the consequent lessened effectiveness of the filter makes this reduced contribution insignificant.

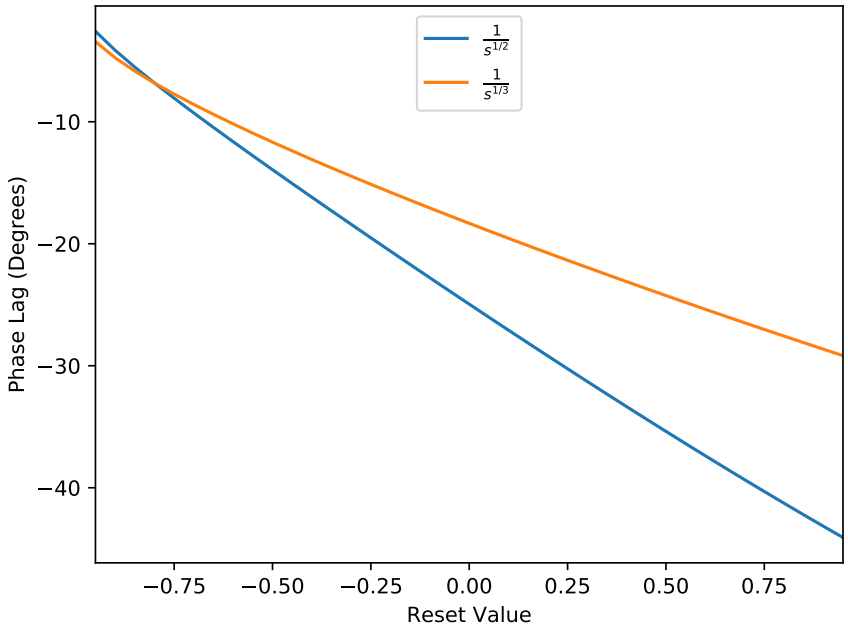

(a) 1st harmonic phase of $\frac{1}{s^{1/2}}$ and $\frac{1}{s^{1/3}}$ for different reset values

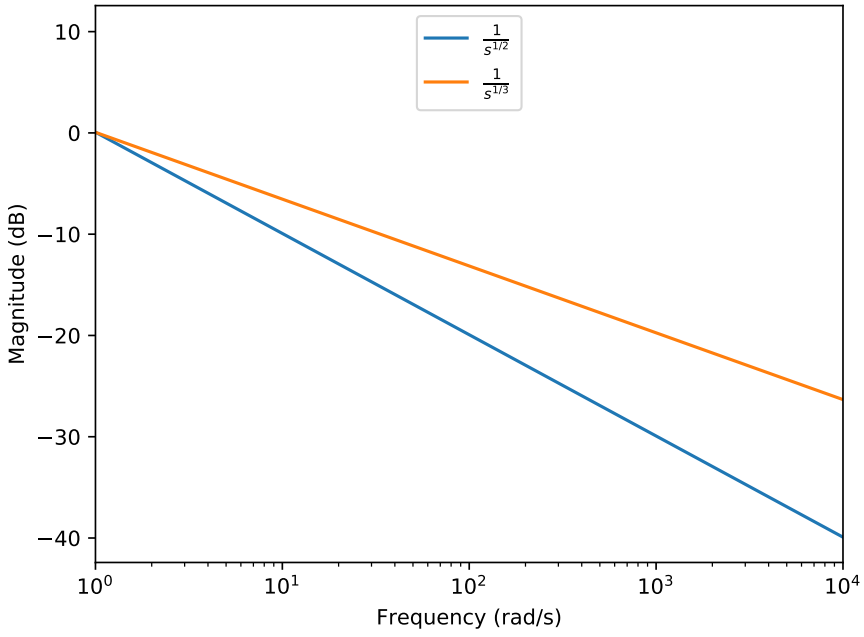

(b) 1st harmonic gain of $\frac{1}{s^{1/2}}$ and $\frac{1}{s^{1/3}}$

B

USE OF LEAD ELEMENT IN THE ANALOGUE

In the paper, the CRONE approximation was used to implement the augmented fractional order analogue. The consequence is that the fractional order analogue will only have the integrating behavior in the specified frequency range, with the gain response flattening outside this range. For an alternative implementation to allow the integrating behavior to act in all frequencies independent of the specified frequency range, the architectures shown in figure B.2 can be used. Here, the use of a traditional Clegg Integrator in the cascade allows for the integrating behavior in the overall response to exist outside the frequency range of the CRONE approximation, with the fractional lead element used to correct the slope in the approximation frequency range. Figure B.1 compares the 1st order harmonic gain of the analogue with and without a lead element implementation; from this figure it's clear that the 1st order gain of the analogue approximates the reset integrator's 1st harmonic much better (albeit not perfect) outside the specified CRONE approximation range, and thus the analogue still has an integrating behavior outside this specified approximation range. This appendix shows the reset values and the corresponding third harmonic reduction for the two element analogue with a fractional lead element, and possible reason behind these values. The architectures and the values are shown in figure B.2 and table B.1.

- An explanation as to why architectures (1) and (2) could not provide a significant reduction is attempted. Optimization results in table B.1 of architectures that have significant 3rd order harmonic gain reduction (i.e. (3) and (6)) show that the filtering integrators (integrator at the end of the cascade) are partially reset, suggesting that the highly reset starting integrator cannot fully provide the required reduced phase lag advantage, and so the filtering integrator also has to support this. Looking at figure B.3, it compares the 3rd order harmonic gain of resetted $\frac{1}{s}$ and $\frac{1}{s^{0.5}}$ for decreasing reset values (i.e. towards $\gamma = -1$). From this figure it is seen that the maximum frequency of the sinusoidal input at which the 3rd order harmonic gain of the traditional integrator is above the fractional integrator in-

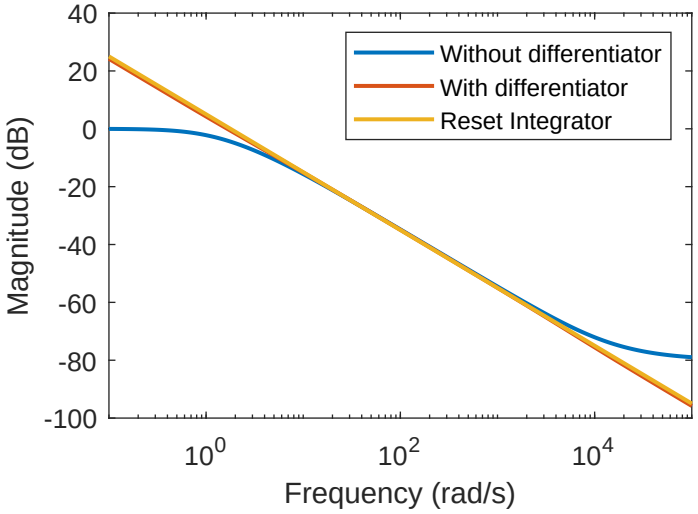

Figure B.1: 1st order harmonic gain of the reset integrator (with reset value of 0) and its analogue with and without differentiator implementation. All fractional elements used are CRONE approximated between 1 and 10000 rad/s.

Architecture	γ_1	γ_2	Third harmonic gain reduction (dB)
(1)	0	1	0.0061
(2)	0	1	0.0050
(3)	-0.9409	0.7122	2.1456
(4)	N/A	N/A	N/A
(5)	N/A	N/A	N/A
(6)	-0.9802	0.8420	2.4644

Table B.1: Third order harmonic reduction for two-element Fractional Clegg Integrator, **lead not reset**; reset of CI = 0

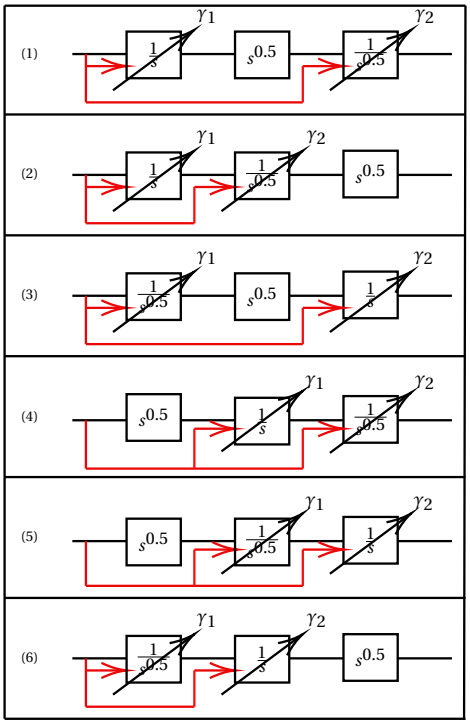

Figure B.2: All possible architectures for a two-element fractional order Clegg Integrator

creases. In addition, looking at the magnitude of the 3rd harmonic in this figure for low γ values (for instance $\gamma = -0.95$), at some frequencies of the sinusoidal input ($\omega < 50 rad/s$), the traditional integrator introduces 3rd order harmonic gain that has an amplitude larger than the sinusoidal input itself (i.e. above 0 dB), whereas the fractional integrator do so at a much smaller frequencies. This means that by using the traditional integrator as the integrator that provides reduced phase lag advantage, there exist more input frequency ranges at which the higher order harmonics is larger than the input amplitude, which translates to more significant higher order harmonics that have to be filtered by a fractional integrator. Looking at the 1st harmonic gain behaviour of the fractional integrator in figure B.4, the less steep negative slope (in comparison to a traditional integrator) means that it has to be linear (i.e. $\gamma = 1$) in order to effectively filter the higher order harmonics, giving no chance to provide the support in providing the reduced phase lag advantage required by the starting integrator. Thus, since the lead and fractional integrator are both linear, they cancel each other, effectively making the cascade only consist of a CI. And since there is a constraint for the cascade to have the same 1st harmonic gain performance as a CI, this CI is then reset to 0, causing no change whatsoever. Although in the table there is a slight 3rd order harmonic gain reduction, it is merely due to the optimizer trying to satisfy the constraints' tolerance at

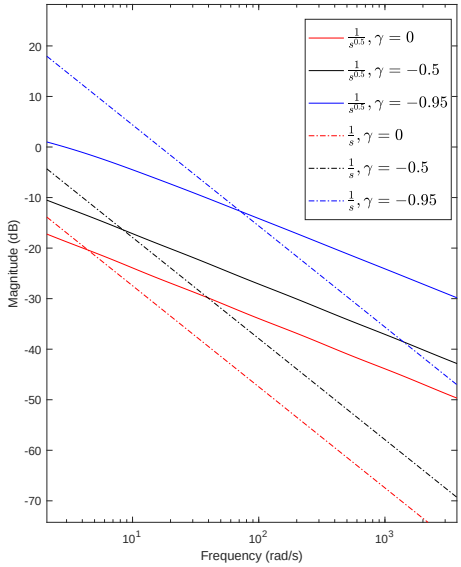

Figure B.3: 3rd harmonic of $\frac{1}{s^{0.5}}$ and $\frac{1}{s}$ for different reset values

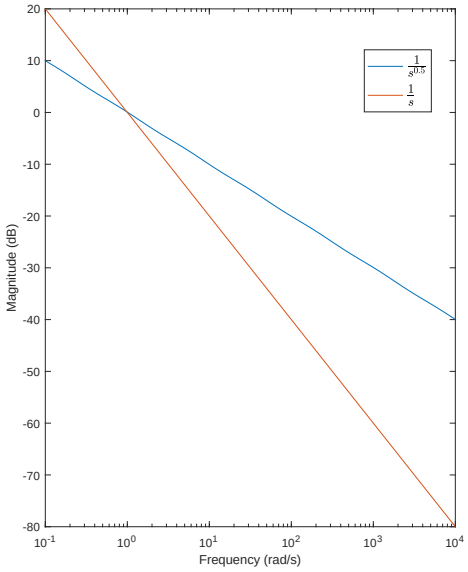

Figure B.4: 1st harmonic of $\frac{1}{s^{0.5}}$ and $\frac{1}{s}$

the boundaries.

- The optimizer could not find a solution for architectures (4) and (5). These architectures have a lead element at the start of the cascade. Figure B.5 illustrates the input and output of the first two elements of these architectures. Here it is observed that the output of the lead element (shown in red) is a 45° shift of its sinusoidal input (shown in blue). This output becomes input into the reset integrator, after which the integrator's output is shown in green. Since the reset of these two architectures are done with respect to input of lead element, the reset instant is as shown in gray dotted line, as opposed to black dotted line which would be the case if reset is with respect to input of integrator. Thus, this causes less phase lag reduction advantage than what could have been achieved. To recoup this loss as well as providing the original required phase lag reduction advantage, this middle integrator might have to be reset lower than -1, which is not allowed in the optimization routine in order to ensure Schur stability. This may very well be the case, in view of the other architectures already requiring the integrator that provide the phase lag reduction advantage (which is reset with respect to its (sinusoidal) input), to have a reset value close to -1.

- In contrast to architectures (1) and (2), architectures (3) and (6) has a traditional integrator as the filtering integrator. Looking at figure B.4, the more negative slope of the first harmonic of $\frac{1}{s}$ means that higher order harmonics can be filtered ef-

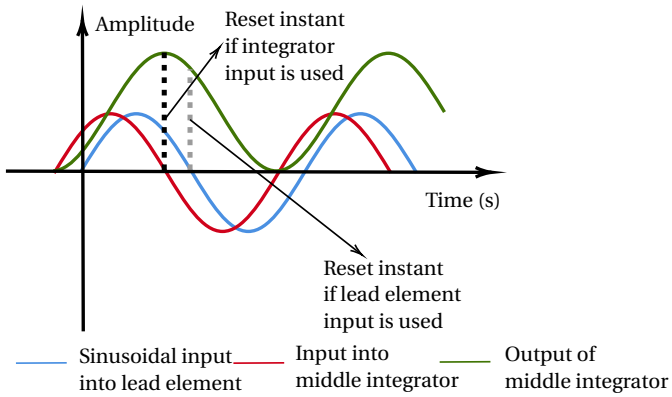

Figure B.5: Illustration of time domain input and output of the first two elements of architecture (4) and (5)

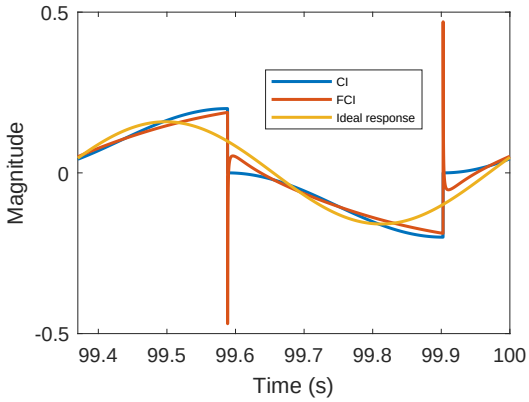

Figure B.6: Output of architecture (6) given input of $\sin(10t)$

fectively without the integrator resorting to becoming fully linear, and thus could also contribute in providing the phase advantage. Comparing these two, (6) has a higher order harmonic reduction compared to (3). However, looking at the simulation output in figure B.6, architecture (6) shows excessive jumping/spikes at the reset instants. In practical implementation, although an LPF or other control elements are used, this behaviour still rises the risk of saturating the actuator.

Given the considerations above, it is then recommended to use architecture (3) as the analogue of the reset integrator for an alternative implementation with a lead element.

C

Effect of PID scheme on Higher Order Harmonics

In the paper, the parallel PID scheme was chosen as opposed to the traditionally series PID scheme used in precision industry. The reason is that with a series configuration, the higher order harmonics output by the reset integrator will pass through the differentiator, which consequently will unnecessarily amplify these higher order harmonics and deteriorate performance. To verify this claim, the open loop response of the series and parallel PID scheme is compared in figure C.2, with each scheme plotted in figure C.1 for clarity. The extra controller C is placed in the specified position so that it specifically acts on the error signal and not on the intermediate signals within the controller. his appendix looks into the possibility of reduced higher order harmonics in a reset controller by placing the differentiator used in a PID controller in parallel configuration, as opposed to putting it in series as was done in illustrative example section of the main paper. It is clear from figure C.2 that the 3rd harmonics of the parallel PID is lower than series, which consequently makes tuning results based on DF more reliable.

To further reduce the effects of higher order harmonics, a notch filter can be applied at the resonance of the plant. Figure C.3 shows the effect of applying the notch filter, with the 3rd order harmonic peak now completely removed and thus the 3rd harmonic is now consistently below the 1st harmonic over all frequency ranges.

The process sensitivity plot for the controllers using parallel PID configuration and a notch filter is plotted in figure C.5. The use of notch filter causes a peak of this disturbance rejection at the resonant frequency of the plant, with the input disturbance now even amplified beyond its initial amplitude for PI+D. This therefore shows that this technique to improve reliability of DF gives a downside of poorer performance in disturbance rejection.

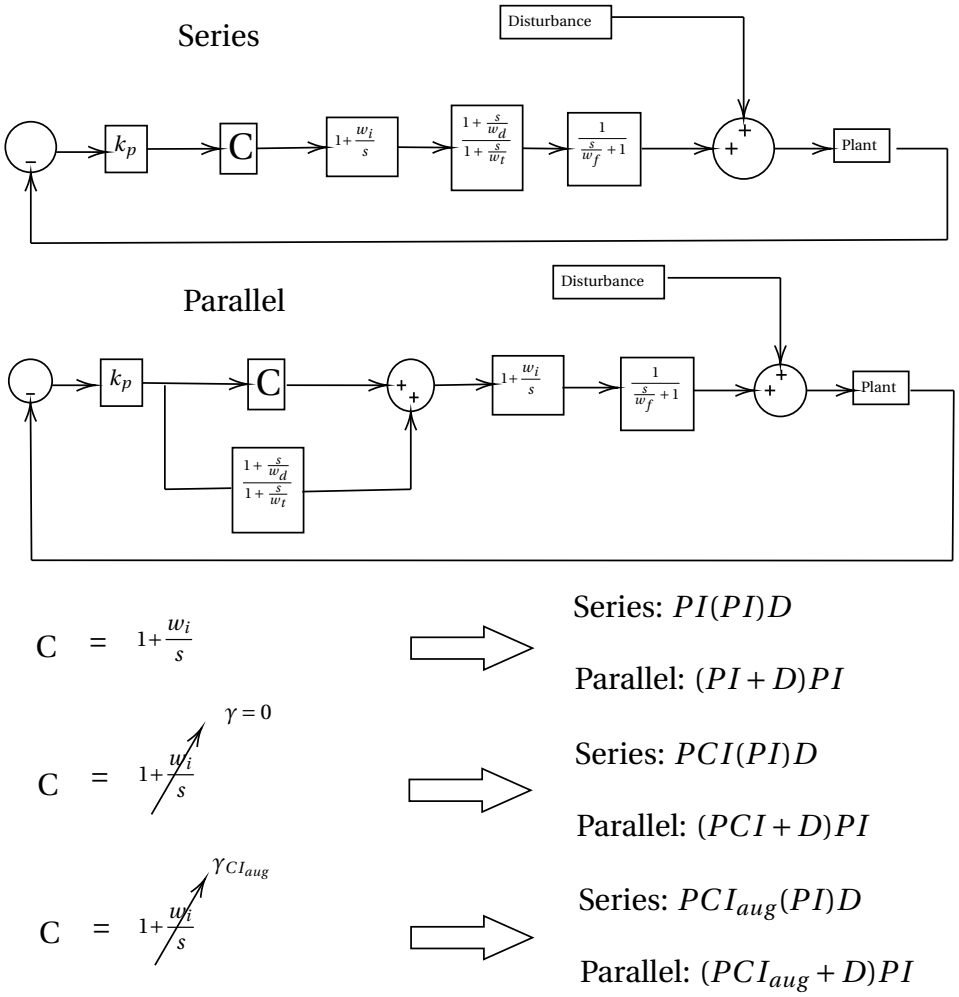

Figure C.1: Series vs. Parallel PID Scheme. C refers to the extra controller alluded to in the paper.

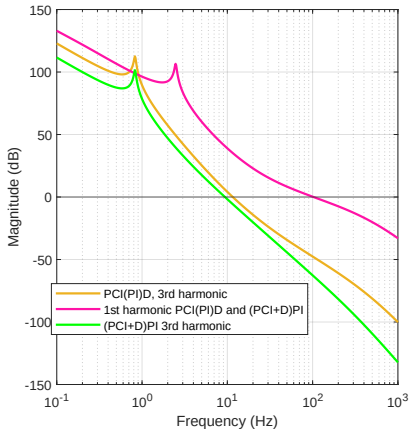

Figure C.2: Comparison of 3rd order harmonic of series and parallel PID

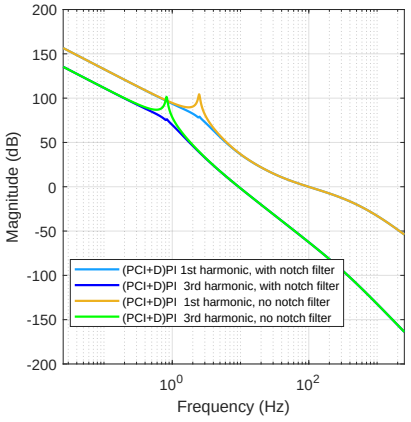

Figure C.3: Comparison of 3rd order harmonic of parallel configuration with and without notch filter applied

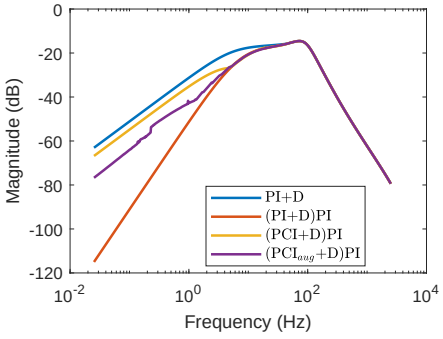

Figure C.4: Process sensitivity of parallel configuration without notch filter

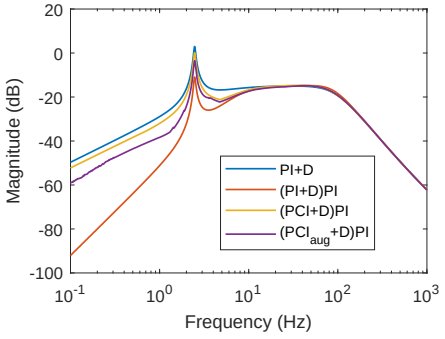

Figure C.5: Process sensitivity of parallel configuration with notch filter

D

PERFORMANCE IMPROVEMENT IN OTHER AREAS

D.1. OPEN LOOP TIME DOMAIN OUTPUT

This section examines the effects of using the analogue to reduce the higher order harmonics in time domain. Figure D.1a compares the output of the Clegg Integrator and the analogue with $p = 2$. From this figure it is seen that the output of the analogue approximates better that of the "ideal" response, this being the first harmonic of the Clegg Integrator. This improvement is seen through the analogue having a smaller integrated squared error (ISE) compared to the Clegg Integrator itself.

D.2. CLOSED LOOP REFERENCE TRACKING

In the paper, only disturbance rejection performance was examined. This section reports the results of simulation for reference tracking of the same control scheme consid-

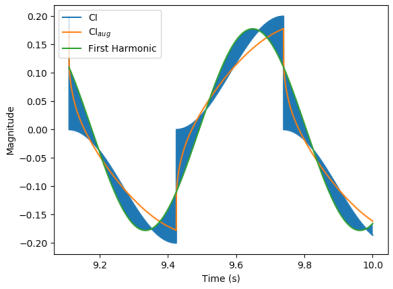

(a) Integrated squared error (ISE) of CI defined as the area between response of CI and ideal response; **ISE = 17.27**

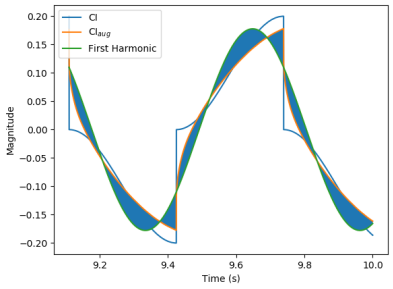

(b) Integrated squared error (ISE) of analogue of CI defined as the area between response of CI's analogue and ideal response; **ISE = 9.01**

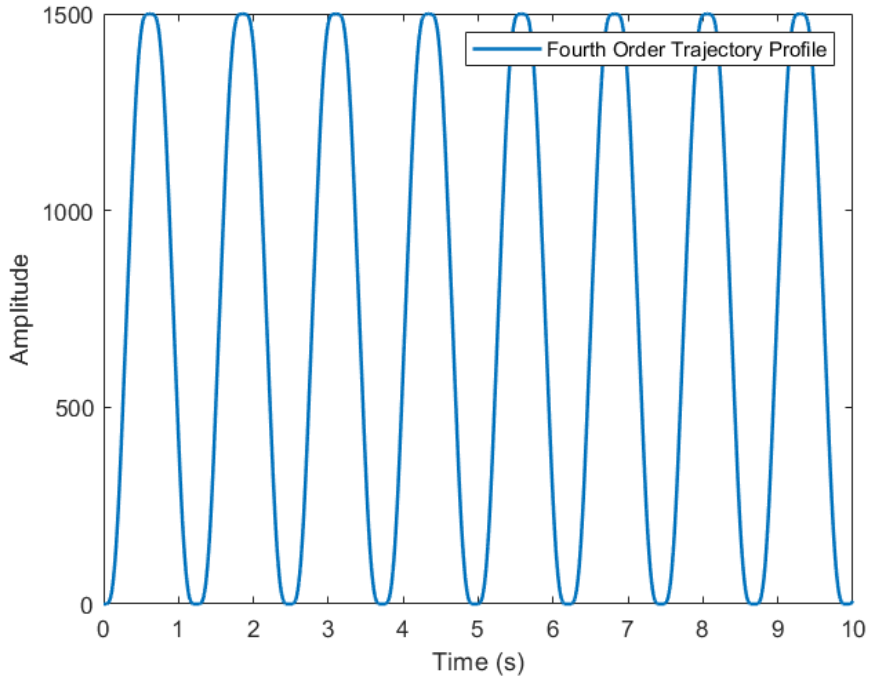

Figure D.2: Fourth order trajectory profile to be followed by the control scheme described in the paper

ered in the paper. Two references were considered. First is a sinusoidal wave of different frequencies, and the second is a fourth-order trajectory profile described by Lamberts et. al. [11] and shown in figure D.2 .

For following sinusoidal reference, (PI+D)PI was found to be able to follow the reference better at all frequencies compared to PI+D and so the results of PI+D are not quoted here for brevity. Therefore, it is desired that the controllers with the reset controller are able to follow the (PI+D)PI's response. Different to the method for disturbance rejection, since the signal to be followed is non-zero, then it is more accurate to calculate the ISE (integrated square error) between the desired signal and the response, rather than only the maximum amplitude of the response and seeing whether its amplitude is equal to the desired response.

The results are shown in table D.1 and D.3. From these data it is seen that the reset controller with the reset controller analogue consistently has lower ISE compared to the controller with the traditional reset integrator. Therefore it is established that performance improvement is also obtained with regards to reference tracking, on top of disturbance rejection.

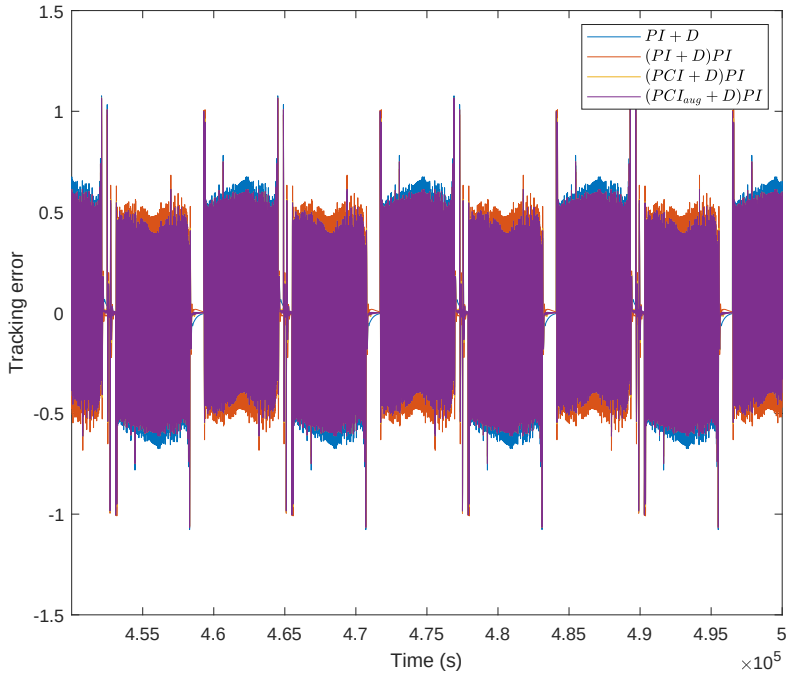

Figure D.3: Fourth order trajectory error. ISE of PI+D = 23.16, (PI+D)PI =21.69, (PCI+D)PI = 21.91, (PCI$_{aug}$+D)PI = 21.87

Input Frequency	ISE of (PCI+D)PI	ISE of (PCI$_{aug}$)+D)PI
0.3	1.0564e-4	7.7042e-5
0.5	3.78e-4	2.5294e-4
0.7	7.8309e-4	6.0032e-4
0.9	0.0012	0.0010
1	0.0016	0.0011
4	8.6511e-4	8.8370e-4
5	0.2661	0.0567
8	10.4130	5.7490
9	20.8173	17.5962
10	4.3032	2.4304

Table D.1: ISE of (PCI+D)PI and (PCI$_{aug}$+D)PI, error is between the respective controller and response of (PI+D)PI

E

System Overview

This section provides the detail of experiment setup used to validate the simulation results

E.1. Setup details

The experimental setup built by Bart Joziasse [3] is used to validate the simulation results; only the fine stage is used. The side view is shown in this figure ... .

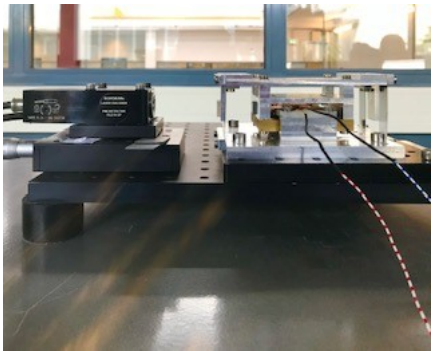

Figure E.1: Fine Stage

The black base is fixed on a vibration isolation table. The encoder used is a Renishaw RLE10 Laser Interferometer with a resolution of 10 nm. The actuator is a copper wire wound 140 times situated between the pairs of parallel flexures shown in figure E.1; it has a diameter of 0.5 mm. The schematic of the experiment is shown in figure E.2.

E.2. System Identification

A chirp signal with frequency ranging from 0.1 Hz to 1000 Hz was used as input for obtaining the frequency response of the setup. The chirp signal frequency increases every

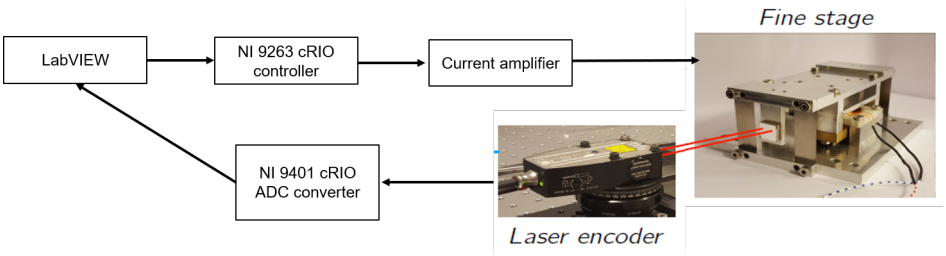

Figure E.2: Schematic of experiment

250ms and the position data is logged every 10μs. The data is then processed using tfestimate function in MATLAB, and tfest is used to obtain the transfer function of the setup:

$$G(s) = \frac{3.038e4}{s^2 + 0.7413s + 243.3} \tag{E.1}$$

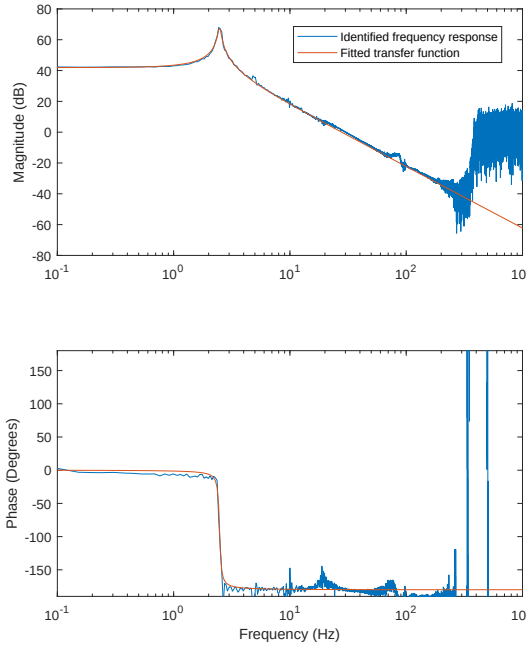

Figure E.3: Frequency response and fitted transfer function

F

STABILITY CHECK

In this chapter, the stability of the fractional order analogue in the disturbance rejection control scheme described in the paper is investigated. The H_β condition as described in the paper is used, utilizing a YALMIP Sedumi solver to solve the LMI in MATLAB. Figure F.1 shows the control scheme with extra information in order to help in understanding the following MATLAB code.

```
%% Check stability code

%ss_total_FCI is the state space of total controller. It has been ...
    constructed
%such that the it corresponds to a state vector, where the first n ...
    entries
%of this state vector belong to the reset integrator (this reset
%part has n states), and the remaining entries belong to the
%differentiator and linear integrator. See diagram below for details

%FIrst build the state space of LPF and plant
ss_LPF=ss(LPF);
ss_plant=ss(-SYS);

%Next put all into a cell:
A_collect{1}=ss_total_FCI.A;
B_collect{1}=ss_total_FCI.B;
C_collect{1}=ss_total_FCI.C;
D_collect{1}=ss_total_FCI.D;

A_collect{2}=ss_LPF.A;
B_collect{2}=ss_LPF.B;
C_collect{2}=ss_LPF.C;
D_collect{2}=ss_LPF.D;

A_collect{3}=ss_plant.A;
B_collect{3}=ss_plant.B;
C_collect{3}=ss_plant.C;
```

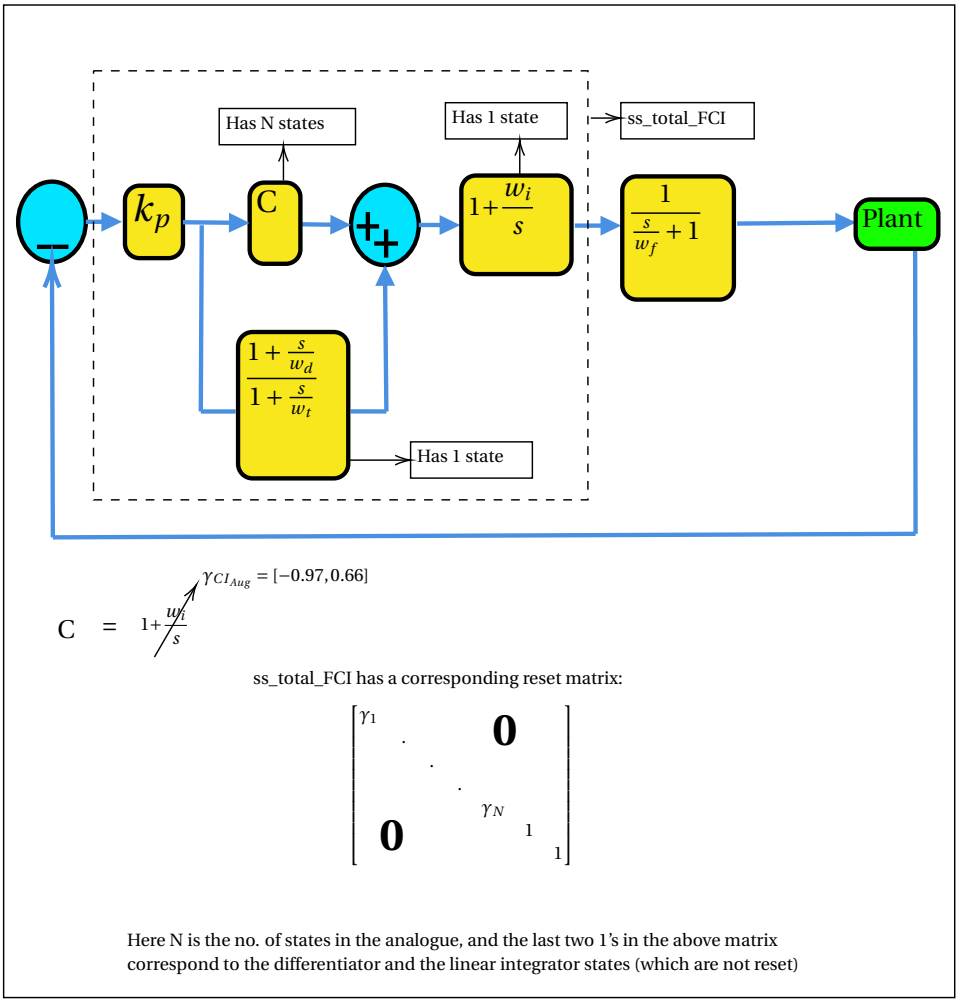

Figure F.1: Extra explanation to help understand the MATLAB code that investigates stability

```
D_collect{3}=ss_plant.D;

%Cascade the controller state space with that of LPF and plant

[A_openloop,B_openloop,C_openloop,D_openloop]=cascadeSSM(A_collect,...
B_collect,C_collect,D_collect);

%Next we build the closed loop state space
syscl=feedback(ss(A_openloop,B_openloop,C_openloop,D_openloop),-1);
%Take the A matrix of this closed loop state space
Acl=syscl.A;

%%
%Now we specify the amount of reset states and non reset states
%for the "equality" part of the Lyapunov condition i.e.
%the B0'P==C0 part.

nrho=9; %no of controller reset states; if there's too many reset states
%then this code may run into numerical issues due to arithmetic with
%numbers that are too small so be careful

nrhobar=3; %no of controller non reset states, including LPF (so D, ...
    linear I and LPF)
np=order(ss_plant); %no of plant states
%%
%Now we build B0 and C0 using the above information
%and specify beta and Prho as objective variable for
%LMI solver

beta=sdpvar(nrho,1,'full','real');
Prho=sdpvar(nrho,nrho,'full','real');
B0=[zeros(np,nrho);zeros(nrhobar,nrho);ones(nrho,nrho)];
C0=[beta*ss_plant.C zeros(nrho,nrhobar) Prho];

%normalize Acl so that we don't run into problems with
%numbers being too small or too large after arithmetic operations
Acl=Acl/norm(Acl);
%%
%For the condition A_rho'PA_rho-P≤0 inequality, need to
%edit A_rho so that we have the (non reset) states of
%the plant and LPF also in it

A_rho_augmented=blkdiag(A_rho_FCI,eye(np+1));% 1 here is the state ...
    of the LPF
%%
%Now specify LMI and constraint equality, and solve for
%P, the objective
P=sdpvar(size(Acl,1),size(Acl,1),'symmetric');

lmi=Acl'*P+P*Acl≤0;
eps=1e-14;
constr=[P≥eps*eye(size(Acl,1)), ...
    B0'*P==C0,A_rho_augmented'*P*A_rho_augmented-P≤0];
ops=sdpsettings('solver','sedumi','verbose',1);

F=solvesdp([lmi constr],0,ops);
%%
```

```
%display P and check if eigenvalues are positive
%if eigenvalues are positive then we have a stable
%controller
if F.problem==0
P
end
```

Running the above MATLAB code returned the following response:

```
P: Linear matrix variable 14x14 (symmetric, real, 105 variables)
Eigenvalues between [1.1111e-10,0.021598]
Coeffiecient range: 1 to 1
```

Since a P is found that has all positive eigenvalues, by the H_β condition the fractional order analogue is stable.

G

MATLAB AND SIMULINK CODE

Here the MATLAB and SIMULINK codes are given.

G.1. OBJ_CHANGE_GAMMA.M

This code runs the objective function for optimizing the reset values for architecture (3) (i.e. Best architecture with lead element).

```
%% This function is the objective function used in the optimization ...
    routine
function [obj]= obj_change_gamma(gamma,CI_reset)
    N=9; %No of poles in the CRONE approximation

    %Specify the range of frequencies where the approximation is valid
    w_lower_wanted=1;%rad/s
    w_higher_wanted=1000*2*pi;%rad/s

    % Number of integrators
    alpha=-1/(length(gamma)-1)*ones(1,(length(gamma)-1));

    % Frequency spacing in logarithmic scale
    freqs = logspace(log10(w_lower_wanted),log10(w_higher_wanted),1000);

    % Translate the valid frequency range into values that the CRONE
    % approximation function takes in
    wl=10^(log10(w_lower_wanted)-0.5);
    wh=10^(log10(w_higher_wanted)+0.5);

    % Initialize reset matrix
    Arho=[];

    % Build state space of each block in the cascade
    for i=1:length(alpha)
        if i==1
            % Build the fractional integrator and lead filter
            tf_block=zz(alpha(i),N,wl,wh);
```

```
28              ss_block=ss(tf_block);
29
30              A_collect{1,i}=ss_block.A;
31              B_collect{1,i}=ss_block.B;
32              C_collect{1,i}=ss_block.C;
33              D_collect{1,i}=ss_block.D;
34
35              syms x;
36              alpha_beda=solve(-1+x==alpha(1));
37              alpha_beda=double(alpha_beda);
38              tf_block=zz(alpha_beda,N,wl,wh);
39              ss_block=ss(tf_block);
40
41              A_collect{1,i+1}=ss_block.A;
42              B_collect{1,i+1}=ss_block.B;
43              C_collect{1,i+1}=ss_block.C;
44              D_collect{1,i+1}=ss_block.D;
45
46          elseif i>1 %build the remaining integrator(s)
47              s=tf('s');
48              A_collect{1,i+1}=ss(1/s).A;
49              B_collect{1,i+1}=ss(1/s).B;
50              C_collect{1,i+1}=ss(1/s).C;
51              D_collect{1,i+1}=ss(1/s).D;
52          end
53
54      % Cascade the state space matrices
55      [Atot,Btot,Ctot,Dtot]=cascadeSSM(A_collect,B_collect,C_collect, ...
            D_collect);
56
57      % Build the reset matrix
58          %Since ss_block is controllable canonical, we reset all the ...
                states not just the end state. If you find it in your ...
                MATLAB to be observable canonical then adapt appropriately
59          if i==1
60            Arho=blkdiag(Arho,diag(gamma(i)*ones(1,length(ss_block.A))));
61            Arho=blkdiag(Arho,diag(gamma(i+1)*ones(1,length(ss_block.A))));
62          elseif i>1
63            Arho=blkdiag(Arho,diag(gamma(i+1)));
64          end
65      end
66
67      %Calculate the 1st and 3rd harmonic gain response
68      sys=ss(Atot,Btot,Ctot,Dtot);
69      HOSIDF_order=[1 3];
70      [Gabs,¬]=hosidf(sys, Arho, HOSIDF_order, ...
71      freqs,0);
72
73  % The 1st harmonic gain responses may have a gain (DC) offset ...
        compared to
74  % the CI. We need to correct for the gain offset.
75  % Compute the gain of CI and find gain that makes the 1st harmonic gain
76  % response equal
77
78      s=tf('s');
79      sys_real=1/s;
80      [real_gain,real_phase]=hosidf(ss(sys_real),CI_reset,HOSIDF_order,...
```

```
81      freqs,0);
82      % The ratio is calculated as the ratio of the responses at the ...
            middle
83      % of the frequency approximation range.
84      ratio=db2mag(real_gain(1,500))/db2mag(Gabs(1,500));
85      % The if statement below is to ensure ratio is always a number
86      if isnan(ratio)
87          ratio=1;
88      end
89      %Now we have the gain offset, apply this to the FCI
90      sys_adjusted=ratio*sys;
91      [Gabs,¬]=hosidf(sys_adjusted, Arho, HOSIDF_order,...
92       freqs,0);
93  %% Finally calculate the objective
94      %The objective is to maximize the difference between the 1st and 3rd
95      %harmonic, which translates to minimizing the third harmonic. Since
96      %the integrator has consistent -1 gradient,  minimizing this ...
            difference
97      %at the middle of the frequency range will also make the same
98      %difference at other frequencies.
99
100     %This objective function was found to be faster and more robust for
101     %different frequency ranges, as opposed to directly minimizing ...
            the 3rd
102     %harmonic.
103     gain_difference=abs(Gabs(1,500)-Gabs(2,500));
104     obj=-gain_difference;
```

G.2. OBJ_CHANGE_GAMMA_NO_LEAD.M

This code runs the objective function for optimizing the reset values for architecture without lead element.

```
1   %% This function is the objective function used in the optimization ...
        routine
2   function [obj]= obj_change_gamma_no_lead(gamma,CI_reset)
3   N=9; %No of poles in the CRONE approximation
4
5   %Specify the range of frequencies where the approximation is valid
6   w_lower_wanted=1;%rad/s
7   w_higher_wanted=1000*2*pi;%rad/s
8
9   % Number of integrators
10  alpha=-1/(length(gamma)-1)*ones(1,(length(gamma)-1));
11
12  % Frequency spacing in logarithmic scale
13  freqs = logspace(log10(w_lower_wanted),log10(w_higher_wanted),1000);
14
15  % Translate the valid frequency range into values that the CRONE
16  % approximation function takes in
17  wl=10^(log10(w_lower_wanted)-0.5);
18  wh=10^(log10(w_higher_wanted)+0.5);
19
20  % Initialize reset matrix
```

```
Arho=[];

% Build state space of each block in the cascade
for i=1:length(alpha)

    % Build the fractional integrator and lead filter
    tf_block=zz(alpha(i),N,wl,wh);
    ss_block=ss(tf_block);

    A_collect{1,i}=ss_block.A;
    B_collect{1,i}=ss_block.B;
    C_collect{1,i}=ss_block.C;
    D_collect{1,i}=ss_block.D;


    % Cascade the state space matrices
    [Atot,Btot,Ctot,Dtot]=cascadeSSM(A_collect,B_collect,C_collect, ...
        D_collect);
    % Build the reset matrix
        %Since ss_block is controllable canonical, we reset all the ...
            states not just the end state. If you find it in your ...
            MATLAB to be observable canonical then adapt appropriately
    Arho=blkdiag(Arho,diag(gamma(i)*ones(1,length(ss_block.A))));
end

%Calculate the 1st and 3rd harmonic gain response
sys=ss(Atot,Btot,Ctot,Dtot);
HOSIDF_order=[1 3];
[Gabs,¬]=hosidf(sys, Arho, HOSIDF_order, ...
freqs,0);

% The 1st harmonic gain responses may have a gain (DC) offset ...
    compared to
% the CI. We need to correct for the gain offset.
% Compute the gain of CI and find gain that makes the 1st harmonic gain
% response equal

s=tf('s');
sys_real=1/s;
[real_gain,real_phase]=hosidf(ss(sys_real),CI_reset,HOSIDF_order,...
freqs,0);
% The ratio is calculated as the ratio of the responses at the middle
% of the frequency approximation range.
ratio=db2mag(real_gain(1,500))/db2mag(Gabs(1,500));
% The if statement below is to ensure ratio is always a number
if isnan(ratio)
ratio=1;
end
%Now we have the gain offset, apply this to the FCI
sys_adjusted=ratio*sys;
[Gabs,¬]=hosidf(sys_adjusted, Arho, HOSIDF_order,...
freqs,0);
%% Finally calculate the objective
%The objective is to maximize the difference between the 1st and 3rd
%harmonic, which translates to minimizing the third harmonic. Since
%the integrator has consistent -1 gradient,  minimizing this difference
%at the middle of the frequency range will also make the same
```

```
%difference at other frequencies.

%This objective function was found to be faster and more robust for
%different frequency ranges, as opposed to directly minimizing the 3rd
%harmonic.
gain_difference=abs(Gabs(1,500)-Gabs(2,500));
obj=-gain_difference;
```

G.3. NLCON_CHANGE_GAMMA.M

This code contains the constraint functions for optimizing the reset values for architecture (3) (i.e. Best architecture with lead element).

```
%% This function is the nonlinear constraint function used in the ...
    optimization routine
function [c,ceq]= nlcon_change_gamma(gamma,CI_reset,special_position)
    N=9; %No of poles in the CRONE approximation

    %Specify the range of frequencies where the approximation is valid
    w_lower_wanted=1;%rad/s
    w_higher_wanted=1000*2*pi;%rad/s

    % Number of integrators
    alpha=-1/(length(gamma)-1)*ones(1,(length(gamma)-1));

    % Frequency spacing in logarithmic scale
    freqs = logspace(log10(w_lower_wanted),log10(w_higher_wanted),1000);

    % Translate the valid frequency range into values that the CRONE
    % approximation function takes in
    wl=10^(log10(w_lower_wanted)-0.5);
    wh=10^(log10(w_higher_wanted)+0.5);

    % Initialize reset matrix
    Arho=[];

    % Build state space of each block in the cascade
    for i=1:length(alpha)
        if i==1
            % Build the fractional integrator and lead filter
            tf_block=zz(alpha(i),N,wl,wh);
            ss_block=ss(tf_block);

            A_collect{1,i}=ss_block.A;
            B_collect{1,i}=ss_block.B;
            C_collect{1,i}=ss_block.C;
            D_collect{1,i}=ss_block.D;

            syms x;
            alpha_beda=solve(-1+x==alpha(1));
            alpha_beda=double(alpha_beda);
            tf_block=zz(alpha_beda,N,wl,wh);
            ss_block=ss(tf_block);

```

```
41              A_collect{1,i+1}=ss_block.A;
42              B_collect{1,i+1}=ss_block.B;
43              C_collect{1,i+1}=ss_block.C;
44              D_collect{1,i+1}=ss_block.D;
45
46          elseif i>1 %build the remaining integrator(s)
47              s=tf('s');
48              A_collect{1,i+1}=ss(1/s).A;
49              B_collect{1,i+1}=ss(1/s).B;
50              C_collect{1,i+1}=ss(1/s).C;
51              D_collect{1,i+1}=ss(1/s).D;
52          end
53
54      % Cascade the state space matrices
55      [Atot,Btot,Ctot,Dtot]=cascadeSSM(A_collect,B_collect,C_collect,...
56      D_collect);
57
58      % Build the reset matrix
59          %Since ss_block is controllable canonical, we reset all the ...
                states not just the end state. If you find it in your ...
                MATLAB to be observable canonical then adapt appropriately
60          if i==1
61            Arho=blkdiag(Arho,diag(gamma(i)*ones(1,length(ss_block.A))));
62            Arho=blkdiag(Arho,diag(gamma(i+1)*ones(1,length(ss_block.A))));
63          elseif i>1
64            Arho=blkdiag(Arho,diag(gamma(i+1)));
65          end
66      end
67
68      %Calculate the 1st and 3rd harmonic gain and phase response
69
70      sys=ss(Atot,Btot,Ctot,Dtot);
71      HOSIDF_order=[1 3];
72      [Gabs,Gphase]=hosidf(sys, Arho, HOSIDF_order, freqs,0);
73
74  % The 1st harmonic gain responses may have a gain (DC) offset ...
        compared to
75  % the CI. We need to correct for this gain offset.
76  % Compute the gain of CI and find gain that makes the 1st harmonic gain
77  % response equal
78
79      s=tf('s');
80      sys_real=1/s;
81      [real_gain,real_phase]=hosidf(ss(sys_real),CI_reset,HOSIDF_order,...
82      freqs,0);
83      % The ratio is calculated as the ratio of the responses at the ...
            middle
84      % of the frequency approximation range.
85      ratio=db2mag(real_gain(1,500))/db2mag(Gabs(1,500));
86      % The if statement below is to ensure ratio is always a number
87      if isnan(ratio)
88          ratio=1;
89      end
90      %Now we have the gain offset, apply this to the FCI. Phase not ...
            needed
91      %to be computed since gain offset does not affect phase
92      sys_adjusted=ratio*sys;
```

```
93      [Gabs,¬]=hosidf(sys_adjusted, Arho, HOSIDF_order, freqs,0);
94
95  %% Finally calculate constraints
96      phase_diff=Gphase(1,500)-real_phase(1,500);
97
98      %The 1st harmonic phase of FCI must be within 0.5 degrees of ...
            that of CI
99      c(1)=phase_diff-0.1;
100     c(2)=-phase_diff-0.1;
101
102     %The gradient of the 1st harmonic gain of FCI must be the same ...
            as that
103     %of CI. This is included because after investigation it was ...
            found that
104     %if each of the reset values used are very negative, the
105     %optimizer could report an optimum reset value that shows a ...
            reduction in
106     %the 3rd harmonic gain at the frequency in middle of the ...
            approximation
107     %range, but however the gradient is not -1 in the range of
108     %approximation. 10^-2 is used to have a more relaxed constraint ...
            and so
109     %the optimization can run faster.
110
111     c(3)=abs((Gabs(1,500)-Gabs(1,499))-(real_gain(1,500)-...
112     real_gain(1,499)))-10^-6;
113
114     %The 3rd harmonic gain of FCI is forced to be less than the 3rd ...
            harmonic gain
115     %of CI
116     c(4)=Gabs(2,500)-real_gain(2,500);
117     ceq=[];
118
119 %         end
120 % else
121 %     return
122 % end
```

G.4. NLCON_CHANGE_GAMMA_NO_LEAD.M

This code contains the constraint functions for optimizing the reset values for architecture without lead.

```
1   %% This function is the nonlinear constraint function used in the ...
        optimization routine
2   function [c,ceq]= ...
        nlcon_change_gamma_no_lead(gamma,CI_reset,special_position)
3   N=9; %No of poles in the CRONE approximation
4
5   %Specify the range of frequencies where the approximation is valid
6   w_lower_wanted=1;%rad/s
7   w_higher_wanted=1000*2*pi;%rad/s
8
9   % Number of integrators
```

```
alpha=-1/(length(gamma)-1)*ones(1,(length(gamma)-1));

% Frequency spacing in logarithmic scale
freqs = logspace(log10(w_lower_wanted),log10(w_higher_wanted),1000);

% Translate the valid frequency range into values that the CRONE
% approximation function takes in
wl=10^(log10(w_lower_wanted)-0.5);
wh=10^(log10(w_higher_wanted)+0.5);

% Initialize reset matrix
Arho=[];

% Build state space of each block in the cascade
for i=1:length(alpha)

    % Build the fractional integrator and lead filter
    tf_block=zz(alpha(i),N,wl,wh);
    ss_block=ss(tf_block);

    A_collect{1,i}=ss_block.A;
    B_collect{1,i}=ss_block.B;
    C_collect{1,i}=ss_block.C;
    D_collect{1,i}=ss_block.D;


    % Cascade the state space matrices
    [Atot,Btot,Ctot,Dtot]=cascadeSSM(A_collect,B_collect,C_collect, ...
        D_collect);
    % Build the reset matrix

    %Since ss_block is controllable canonical, we reset all the ...
        states not just the end state. %If you find it in your ...
        MATLAB to be observable canonical then adapt appropriately
    Arho=blkdiag(Arho,diag(gamma(i)*ones(1,length(ss_block.A))));
end
%Calculate the 1st and 3rd harmonic gain and phase response

sys=ss(Atot,Btot,Ctot,Dtot);
HOSIDF_order=[1 3];
[Gabs,Gphase]=hosidf(sys, Arho, HOSIDF_order, freqs,0);

% The 1st harmonic gain responses may have a gain (DC) offset ...
    compared to
% the CI. We need to correct for this gain offset.
% Compute the gain of CI and find gain that makes the 1st harmonic gain
% response equal

s=tf('s');
sys_real=1/s;
[real_gain,real_phase]=hosidf(ss(sys_real),CI_reset,HOSIDF_order,...
freqs,0);
% The ratio is calculated as the ratio of the responses at the middle
% of the frequency approximation range.
ratio=db2mag(real_gain(1,500))/db2mag(Gabs(1,500));
% The if statement below is to ensure ratio is always a number
if isnan(ratio)
```

```
ratio=1;
end
%Now we have the gain offset, apply this to the FCI. Phase not needed
%to be computed since gain offset does not affect phase
sys_adjusted=ratio*sys;
[Gabs,¬]=hosidf(sys_adjusted, Arho, HOSIDF_order, freqs,0);

%% Finally calculate constraints
phase_diff=Gphase(1,500)-real_phase(1,500);

%The 1st harmonic phase of FCI must be within 0.5 degrees of that of CI
c(1)=phase_diff-0.1;
c(2)=-phase_diff-0.1;

%The gradient of the 1st harmonic gain of FCI must be the same as that
%of CI. This is included because after investigation it was found that
%if each of the reset values used are very negative, the
%optimizer could report an optimum reset value that shows a ...
    reduction in
%the 3rd harmonic gain at the frequency in middle of the approximation
%range, but however the gradient is not -1 in the range of
%approximation. 10^-2 is used to have a more relaxed constraint and so
%the optimization can run faster.

c(3)=abs((Gabs(1,500)-Gabs(1,499))-(real_gain(1,500)-...
real_gain(1,499)))-10^-6;

%The 3rd harmonic gain of FCI is forced to be less than the 3rd ...
    harmonic gain
%of CI
c(4)=Gabs(2,500)-real_gain(2,500);
ceq=[];

%         end
% else
%     return
% end
```

G.5. RUN_CHANGE_GAMMA.M

This function runs the objective and constraint functions above using the fmincon algorithm.

```
function ...
    [X,FVAL]=run_change_gamma(gamma_initial,CI_reset,special_position)
   objective=@(gamma)obj_change_gamma(gamma,CI_reset,special_position);

   A=[];
   b=[];
   Aeq=[];
   Beq=[];
   lb=-1*(ones(length(gamma_initial),1));
   ub=1*(ones(length(gamma_initial),1));
   nonlincon=@(gamma)nlcon_change_gamma(gamma,CI_reset,special_position);
```

```
    options=optimoptions(@fmincon,'Algorithm','sqp','Display','iter');
    [X,FVAL]=fmincon(objective,gamma_initial,A,b,Aeq,Beq,lb,ub,...
    nonlincon,options);

end
```

G.6. OPTIMIZE_ARCHITECTURE.M

This function optimizes architecture (3) for a given reset value of CI.

```
function [X,reduction_in_3rd_harmonic]=optimize_architecture(CI_reset)
    warning OFF
    gamma_initial=[0 0 0];%This specifies the reset values for each ...
        block
    %%
    sets=[];
    for i=1:size(gamma_initial,1)
        [X,FVAL]=run_change_gamma(gamma_initial(i,:),CI_reset,...
        special_position);
        sets(i,:)=[gamma_initial(i,:) X FVAL];
    end
    s=tf('s');
    freqs=logspace(-1,4,1000);
    [Gabs,Gphase]=hosidf(ss(1/s), CI_reset,[1 3],freqs,0);
    FVAL_original=Gabs(1,length(freqs)/2)-Gabs(2,length(freqs)/2);
    reduction_in_3rd_harmonic=abs(abs(FVAL)-abs(FVAL_original));
end
```

G.7. PHASE_MANIPULATION_INVESTIGATION.M

This function calculates the RMS error of FCI with architecture (3) for a given equal phase of the higher order harmonics.

```
%% Higher order harmonics phase manipulation
% This code calculates the RMSE of FCI given that the higher order
% harmonics phase are kept the same, with this phase being changed ...
    from 0
% to -90 degrees
clear
phase_offset=deg2rad(-90:0.1:0);
rms=[];
for i=1:length(phase_offset)
    rms(i)=rms_phase_manipulation_all_phase_same(phase_offset(i));
end
rms_min=min(rms);
phase_offset_best=rad2deg(phase_offset(find(abs(rms-rms_min)<eps)));
%% Plot the results
t=0:0.001:5;
figure;
plot(rad2deg(phase_offset),rms);
title('Phase offset (degrees) vs. rms');
xlabel('Degrees');
```

```
19 ylabel('rms');
20 hold on;
21
22 % The following lines are the gains and phase of the FCI at 10 ...
       rad/s; the
23 % corresponding FCI architecture is as shown in the chapter
24 first_harmonic_phase=deg2rad(-38.89);
25 third_harmonic_phase_ori=deg2rad(-29.17);
26 fifth_harmonic_phase_ori=deg2rad(-27.33);
27 seventh_harmonic_phase_ori=deg2rad(-25.79);
28 ninth_harmonic_phase_ori=deg2rad(-24.47);
29 eleventh_harmonic_phase_ori=deg2rad(-23.4);
30 thirteenth_harmonic_phase_ori=deg2rad(-22.53);
31 fifteenth_harmonic_phase_ori=deg2rad(-21.81);
32 seventeenth_harmonic_phase_ori=deg2rad(-21.19);
33 nineteenth_harmonic_phase_ori=deg2rad(-20.63);
34 twentyfirst_harmonic_phase_ori=deg2rad(-20.12);
35 twentythird_harmonic_phase_ori=deg2rad(-19.65);
36 twentyfifth_harmonic_phase_ori=deg2rad(-19.22);
37 twentyseventh_harmonic_phase_ori=deg2rad(-18.81);
38
39 first_harmonic_gain=db2mag(-15.97);
40 third_harmonic_gain=db2mag(-29.74);
41 fifth_harmonic_gain=db2mag(-35.63);
42 seventh_harmonic_gain=db2mag(-39.47);
43 ninth_harmonic_gain=db2mag(-42.28);
44 eleventh_harmonic_gain=db2mag(-44.49);
45 thirteenth_harmonic_gain=db2mag(-46.31);
46 fifteenth_harmonic_gain=db2mag(-47.68);
47 seventeenth_harmonic_gain=db2mag(-49.21);
48 nineteenth_harmonic_gain=db2mag(-50.4);
49 twentyfirst_harmonic_gain=db2mag(-51.47);
50 twentythird_harmonic_gain=db2mag(-52.43);
51 twentyfifth_harmonic_gain=db2mag(-53.32);
52 twentyseventh_harmonic_gain=db2mag(-54.13);
53
54 y_offset_harmonic_kept_original = ...
55 first_harmonic_gain*sin(10*t+first_harmonic_phase) + ...
56 third_harmonic_gain*sin(3*10*t+ third_harmonic_phase_ori)+ ...
57 fifth_harmonic_gain*sin(5*10*t + fifth_harmonic_phase_ori)+ ...
58 seventh_harmonic_gain*sin(7*10*t+ seventh_harmonic_phase_ori)+ ...
59 ninth_harmonic_gain*sin(9*10*t+ ninth_harmonic_phase_ori)+ ...
60 eleventh_harmonic_gain*sin(11*10*t+ eleventh_harmonic_phase_ori)+ ...
61 thirteenth_harmonic_gain*sin(13*10*t+ ...
       thirteenth_harmonic_phase_ori)+ ...
62 fifteenth_harmonic_gain*sin(15*10*t+ fifteenth_harmonic_phase_ori)+ ...
63 seventeenth_harmonic_gain*sin(17*10*t+ ...
       seventeenth_harmonic_phase_ori)+ ...
64 nineteenth_harmonic_gain*sin(19*10*t+ ...
       nineteenth_harmonic_phase_ori)+ ...
65 twentyfirst_harmonic_gain*sin(21*10*t+ ...
       twentyfirst_harmonic_phase_ori)+ ...
66 twentythird_harmonic_gain*sin(23*10*t+ ...
       twentythird_harmonic_phase_ori)+ ...
67 twentyfifth_harmonic_gain*sin(25*10*t+ ...
       twentyfifth_harmonic_phase_ori)+ ...
68 twentyseventh_harmonic_gain*sin(27*10*t+ ...
```

```
    twentyseventh_harmonic_phase_ori);

%These are the ideal response's gain and phase at 10 rad/s
first_harmonic_gain=db2mag(-15.97);
ideal_response=first_harmonic_gain*sin(10*t+first_harmonic_phase);

%Calculate RMS of original FCI and plot
rms_FCI_original=sqrt(sum((ideal_response-...
y_offset_harmonic_kept_original).^2)/length(ideal_response));
plot(rms_FCI_original,'o');

title('Phase offset (degrees) vs. RMS Error');
xlabel('Degrees');
ylabel('RMS Error');
hold on;
legend('Phase offset','RMS of original FCI')

%% This function calculates the RMS error of FCI for a given phase ...
    offset
%  This function assumes that all the higher order harmonics phase ...
    are the
%  same
function rms=rms_phase_manipulation_all_phase_same(phase_offset)
% Gain of ideal response
CI_first_harmonic_gain=db2mag(-15.97);

% Gains of FCI; architecture used are as shown in the corresponding
% chapter
first_harmonic_gain=db2mag(-15.97);
third_harmonic_gain=db2mag(-29.74);
fifth_harmonic_gain=db2mag(-35.63);
seventh_harmonic_gain=db2mag(-39.47);
ninth_harmonic_gain=db2mag(-42.28);
eleventh_harmonic_gain=db2mag(-44.49);
thirteenth_harmonic_gain=db2mag(-46.31);
fifteenth_harmonic_gain=db2mag(-47.68);
seventeenth_harmonic_gain=db2mag(-49.21);
nineteenth_harmonic_gain=db2mag(-50.4);
twentyfirst_harmonic_gain=db2mag(-51.47);
twentythird_harmonic_gain=db2mag(-52.43);
twentyfifth_harmonic_gain=db2mag(-53.32);
twentyseventh_harmonic_gain=db2mag(-54.13);
% First harmonic phase
first_harmonic_phase=deg2rad(-38.89);

%calculate time responses
t=0:0.001:5;

ideal_response=CI_first_harmonic_gain*sin(10*t+first_harmonic_phase);
%y=[];

y_offset=first_harmonic_gain*sin(10*t+first_harmonic_phase) + ...
  third_harmonic_gain*sin(3*10*t+ phase_offset)+ ...
  fifth_harmonic_gain*sin(5*10*t + phase_offset)+ ...
  seventh_harmonic_gain*sin(7*10*t+ phase_offset)+ ...
  ninth_harmonic_gain*sin(9*10*t+ phase_offset)+ ...
  eleventh_harmonic_gain*sin(11*10*t+ phase_offset)+ ...
```

```
123   thirteenth_harmonic_gain*sin(13*10*t+ phase_offset)+ ...
124   fifteenth_harmonic_gain*sin(15*10*t+ phase_offset)+ ...
125   seventeenth_harmonic_gain*sin(17*10*t+ phase_offset)+ ...
126   nineteenth_harmonic_gain*sin(19*10*t+ phase_offset)+ ...
127   twentyfirst_harmonic_gain*sin(21*10*t+ phase_offset)+ ...
128   twentythird_harmonic_gain*sin(23*10*t+ phase_offset)+ ...
129   twentyfifth_harmonic_gain*sin(25*10*t+ phase_offset)+ ...
130   twentyseventh_harmonic_gain*sin(27*10*t+ phase_offset);
131
132 % Calculate RMS
133 rms=sqrt(sum((ideal_response-y_offset).^2)/length(ideal_response));
134 end
```

G.8. PROCESS_SENSITIVITY.M

This code tunes and calculate the parameters for the four controllers used for disturbance rejection.

```
1  %% Tuning script
2  % This script tunes the 4 controllers in closed loop and also calculates
3  % the discrete state space representation of the controllers for ...
       simulation
4
5  % [T,f]=tfestimate(u,y,[],[],[],1e4);
6  %
7  %DATA=iddata(y,u,Ts);
8  %SYS = tfest(DATA, 2,0);
9  clear
10 close all
11 load('SYS.mat')
12 warning off
13 %% set parameters
14 wh=50000;
15 wl=0.05;
16 wl=10^(log10(wl)-0.5);
17 wh=10^(log10(wh)+0.5);
18 freqs_crone=logspace(log10(wl),log10(wh),1000);
19 [freq index_low] = min(abs(freqs_crone-wl*10));
20 [freq2 index_high] = min(abs(freqs_crone-wh/10));
21 freqs=freqs_crone(index_low:index_high);
22
23 CI_reset=0;
24 no_of_chunks=2;
25 specify_reset=[-0.9409 1 0.7122];
26 %Here I use the architecture with lead, but using the architecture ...
       without lead also produces same result. I use architecture with ...
       lead here because I spent so much time working on it and is so ...
       happy that it works that I use it here instead of the one ...
       without lead.
27 Ts=1e-4;
28 SYS_discrete=c2d(SYS,Ts,'tustin');
29
30 alpha=-1/no_of_chunks*ones(1,no_of_chunks);
31 N=9;
```

```
32
33  s=tf('s');
34  P_rule_of_thumb=1/db2mag(-22)/3.5;
35
36  P=P_rule_of_thumb;
37
38  f_bw=100;
39  w_bw=2*pi*f_bw;
40  wf=w_bw*10;
41  wi=w_bw/10;
42  a=3;
43  wt=w_bw*a;
44  wd=w_bw/a;
45
46  %% Evaluate plant at freqs
47  plant_abs=mag2db(abs(squeeze(freqresp(-SYS,freqs))));
48  plant_phase=rad2deg(unwrap(phase(squeeze(freqresp(-SYS,freqs)))));
49  %% Evaluate LPF at freqs AND ADD TO PLANT
50  LPF=(1/(s/(wf)+1));
51  LPF_discrete=c2d(LPF,Ts,'tustin');
52  %LPF_discrete.num{1}/LPF_discrete.num{1}(1)
53  %LPF_discrete.den{1}
54  LPF_abs=mag2db(abs(squeeze(freqresp(LPF,freqs))));
55  LPF_phase=rad2deg(unwrap(phase(squeeze(freqresp(LPF,freqs)))));
56
57  plant_and_LPF_abs=plant_abs+LPF_abs;
58  plant_and_LPF_phase=LPF_phase+plant_phase;
59
60  %% PI+D
61
62  PID=P *((1+wi/s) + (1+s/wd) / (1+s/wt));
63  %* (1/(s/(wf)+1));
64  P_PID=P;
65  I_PID=(1+wi/s);
66  I_PID_discrete=c2d(I_PID,Ts,'tustin');
67  %I_PID_discrete.num{1}/I_PID_discrete.num{1}(1)
68  %I_PID_discrete.num{1}(1)
69  %I_PID_discrete.den{1}
70  D_PID=(1+s/wd) / (1+s/wt);
71  D_PID_discrete=c2d(D_PID,Ts,'tustin');
72  ss_D_PID=ss(D_PID);
73  %D_PID_discrete.num{1}/D_PID_discrete.num{1}(1)
74  %D_PID_discrete.num{1}(1)
75  %D_PID_discrete.den{1}
76
77  PID_abs=mag2db(abs(squeeze(freqresp(PID,freqs))));
78  PID_phase=rad2deg(unwrap(phase(squeeze(freqresp(PID,freqs)))));
79
80  % For simulation
81  Ts=1e-4;
82  PID_discrete=c2d(PID,Ts,'tustin');
83  %PID_discrete_combine_with_LPF=c2d(PID,Ts,'tustin');
84  %% PI2+D
85  extra_integrator=(1+wi/s);
86  extra_integrator_discrete=c2d((1+wi/s),Ts,'tustin');
87
88  PID_I2D=P *((1+wi/s) + (1+s/wd) / (1+s/wt))*extra_integrator;
```

```
89
90  PI2D_abs=mag2db(abs(squeeze(freqresp(PID_I2D,freqs))));
91  PI2D_phase=rad2deg(unwrap(phase(squeeze(freqresp(PID_I2D,freqs)))));
92
93  PID_I2D_discrete=c2d(PID_I2D,Ts,'tustin');
94  %% CI
95  P_CI=P*1.055;
96  I_CI=(1+wi/s)/1.62;
97  I_CI_discrete=c2d(I_CI,Ts,'tustin');
98  ss_I_CI_discrete=ss(I_CI_discrete);
99  I_CI=ss(I_CI);
100 I_CI_discrete_not_tamed=c2d(ss(1/s),Ts,'tustin');
101
102 %Combine state space of differentiator and reset integrator
103 A_total=blkdiag(I_CI.A,ss_D_PID.A);
104 B_total=[I_CI.B;ss_D_PID.B];
105 C_total=[I_CI.C ss_D_PID.C];
106 D_total=I_CI.D+ss_D_PID.D;
107
108 %Combine state space of P+CI with extra integrator
109
110 ss_extra_integrator=ss(extra_integrator);
111 A_collect={A_total,ss_extra_integrator.A};
112 B_collect={B_total,ss_extra_integrator.B};
113 C_collect={C_total,ss_extra_integrator.C};
114 D_collect={D_total,ss_extra_integrator.D};
115
116 [A_total2,B_total2,C_total2,D_total2]=cascadeSSM(A_collect,B_collect,...
117 C_collect,D_collect);
118
119 ss_total2=P_CI*ss(A_total2,B_total2,C_total2,D_total2);
120 ss_total_PCIID_discrete=c2d(ss_total2,Ts,'tustin');
121 %construct appropriate A_rho
122 diag_of_A_rho=[zeros(1,size(I_CI.A,1)) ...
        ones(1,size(A_total2,1)-size(I_CI.A,1))];
123 A_rho=diag(diag_of_A_rho);
124
125 %HOSIDF it
126 [Gabs_CI,Gphase_CI]=hosidf(ss_total2, A_rho, 1, freqs, 0);
127
128 %% FCI parameters
129
130 %Calculate the state space of the FCI
131 [ratio,FCI_A,FCI_B,FCI_C,FCI_D,Arho]= ...
        find_ratio_better_arch_arch_3(alpha,specify_reset,CI_reset,N,wl,..
132 wh,freqs_crone);
133 ss_FCI2=(1+ss(FCI_A,FCI_B,FCI_C,FCI_D)*wi)/1.62;
134 ss_FCI2_discrete=c2d(ss_FCI2,Ts,'tustin');
135 ss_FCI_discrete_open_loop=c2d(ss(FCI_A,FCI_B,FCI_C,FCI_D),Ts,'tustin');
136
137 %The below is for Labview experiment
138 %Use the state space representation (in Labview) that have elements
139 %that are not smaller than the resolution of digits in Labview
140
141 [num,den]=ss2tf(ss_FCI2.A,ss_FCI2.B,ss_FCI2.C,ss_FCI2.D);
142 ss_FCI2_discrete_labview=c2d(tf(num,den),Ts,'tustin');
143 ss_FCI2_discrete_labview=ss(ss_FCI2_discrete_labview);
```

```
144
145 ss_FCI2_discrete_A=reshape((ss_FCI2_discrete_labview.A)',1,361);
146 ss_FCI2_discrete_B=(ss_FCI2_discrete_labview.B)';
147 ss_FCI2_discrete_C=(ss_FCI2_discrete_labview.C);
148 ss_FCI2_discrete_D=(ss_FCI2_discrete_labview.D);
149
150 ss_FCI2_discrete_A_modal=reshape((canon(ss_FCI2_discrete,'modal').A)',...
151 1,361);
152 ss_FCI2_discrete_B_modal=(canon(ss_FCI2_discrete,'modal').B)';
153 ss_FCI2_discrete_C_modal=(canon(ss_FCI2_discrete,'modal').C);
154 ss_FCI2_discrete_D_modal=(canon(ss_FCI2_discrete,'modal').D);
155 %Calculate P+FCI
156
157 A_total=blkdiag(ss_FCI2.A,ss_D_PID.A);
158 B_total=[ss_FCI2.B;ss_D_PID.B];
159 C_total=[ss_FCI2.C ss_D_PID.C];
160 D_total=[ss_FCI2.D+ss_D_PID.D];
161
162 % Cascade P+FCI with extra I
163 A_collect={A_total,ss_extra_integrator.A};
164 B_collect={B_total,ss_extra_integrator.B};
165 C_collect={C_total,ss_extra_integrator.C};
166 D_collect={D_total,ss_extra_integrator.D};
167
168 [A_total2,B_total2,C_total2,D_total2]=cascadeSSM(A_collect,B_collect,...
169 C_collect,D_collect);
170
171 ss_total_FCI=P_CI*ss(A_total2,B_total2,C_total2,D_total2);
172 %construct A_rho_FCI
173 diag_of_rest_of_Arho=[ones(1,size(A_total2,1)-size(Arho,1))];
174 A_rho_FCI=blkdiag(Arho,diag(diag_of_rest_of_Arho));
175
176 %HOSIDF 'em
177 [Gabs_FCI,Gphase_FCI]=hosidf(ss_total_FCI, A_rho_FCI, 1, freqs, 0);
178
179 % A=ss_FCI2_discrete.A;
180 % A=A';
181 % %A=reshape(A,361,1);
182 % B=ss_FCI2_discrete.B;
183 % C=ss_FCI2_discrete.C;
184 % D=ss_FCI2_discrete.D;
185 % gamma=diag(Arho);
186
187 % A=ss_FCI2_discrete.A;
188 % A=A';
189 % %A=reshape(A,361,1);
190 % B=ss_FCI2_discrete.B;
191 % C=ss_FCI2_discrete.C;
192 % D=ss_FCI2_discrete.D;
193 % gamma=diag(Arho);
194 % Plot 1st harmonic of CI at 10 rad/s
195
196 %% Cascade frequency responses
197
198 Gabs_PID_openloop=PID_abs'+plant_and_LPF_abs';
199 Gphase_PID_openloop=PID_phase'+plant_and_LPF_phase';
200
```

```
Gabs_PI2D_openloop=PI2D_abs'+plant_and_LPF_abs';
Gphase_PI2D_openloop=PI2D_phase'+plant_and_LPF_phase';

Gabs_PCIID_openloop=Gabs_CI+plant_and_LPF_abs';
Gphase_PCIID_openloop=Gphase_CI+plant_and_LPF_phase';

Gabs_PFCIID_openloop=Gabs_FCI+plant_and_LPF_abs';
Gphase_PIFCID_openloop=Gphase_FCI+plant_and_LPF_phase';
%% Evaluate open loop of the different controllers
freqs=freqs./(2*pi);
figure
ax1=subplot(2,1,1);
semilogx(freqs,Gabs_PID_openloop,'LineWidth',1.5);
title('Open loop freq resp, different controllers')
grid on
hold on
semilogx(freqs,Gabs_PI2D_openloop,'LineWidth',1.5);hold on
semilogx(freqs,Gabs_PCIID_openloop,'LineWidth',1.5);hold on
semilogx(freqs,Gabs_PFCIID_openloop,'LineWidth',1.5);
grid on
yline(0);
xlabel('Frequency (Hz)')
ylabel('Magnitude (dB)')
Legend{1}='PID';
Legend{2}='PI2D';
Legend{3}='PCIID';
Legend{4}='PFCIID';
legend(Legend)
%xlim([freqs(1) freqs(end)]);
xlim([0.1 1000])
%ylim([-0.1 0.1]);
hold on

ax2=subplot(2,1,2);
semilogx(freqs,Gphase_PID_openloop,'LineWidth',1.5);

hold on
semilogx(freqs,Gphase_PI2D_openloop,'LineWidth',1.5);hold on
semilogx(freqs,Gphase_PCIID_openloop,'LineWidth',1.5);hold on
semilogx(freqs,Gphase_PIFCID_openloop,'LineWidth',1.5);hold on
grid on
xlabel('Frequency (Hz)')
ylabel('Phase (degrees)')
%yline(-180);
%yline(-135);
xlim([freqs(1) freqs(end)]);
hold off
b=axes('position',[.60 .145 .15 .15]);
indexOfInterest = ...
    numel(find((freqs-95)<eps)):1:numel(find((freqs-105)<eps));
semilogx(freqs(indexOfInterest),Gphase_PID_openloop(indexOfInterest),...
'LineWidth',1.5);hold on % plot on new axes
semilogx(freqs(indexOfInterest),Gphase_PI2D_openloop(indexOfInterest),...
'LineWidth',1.5);hold on % plot on new axes
semilogx(freqs(indexOfInterest),Gphase_PCIID_openloop(indexOfInterest),...
'LineWidth',1.5);hold on % plot on new axes
semilogx(freqs(indexOfInterest),Gphase_PIFCID_openloop(indexOfInterest),...
```

```
257  'LineWidth',1.5);hold on % plot on new axes
258  grid on
259  %axis on
260  set(b,'xticklabel',[]);
261  set(b,'yticklabel',[]);
262  box on
263  ylim([-153 -145])
```

G.9. SIMULINK DIAGRAM FOR DISTURBANCE REJECTION INVESTIGATION

The following diagram shows the Simulink Model used for closed loop validation of the augmented analogue controller.

Overall Simulink simulation:

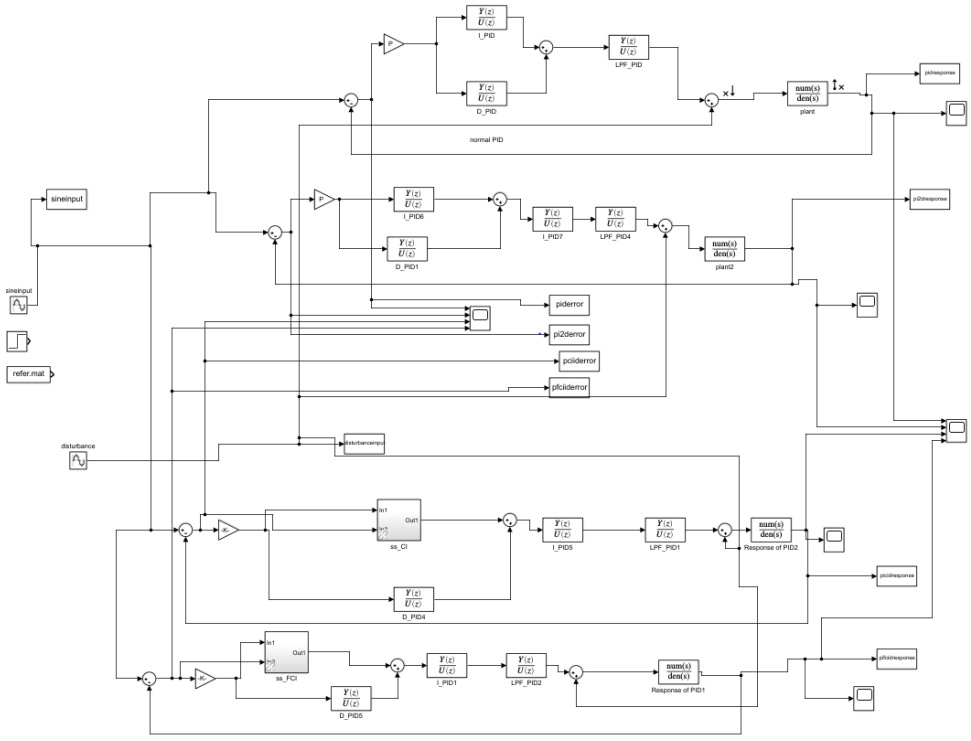

Reset controller block:

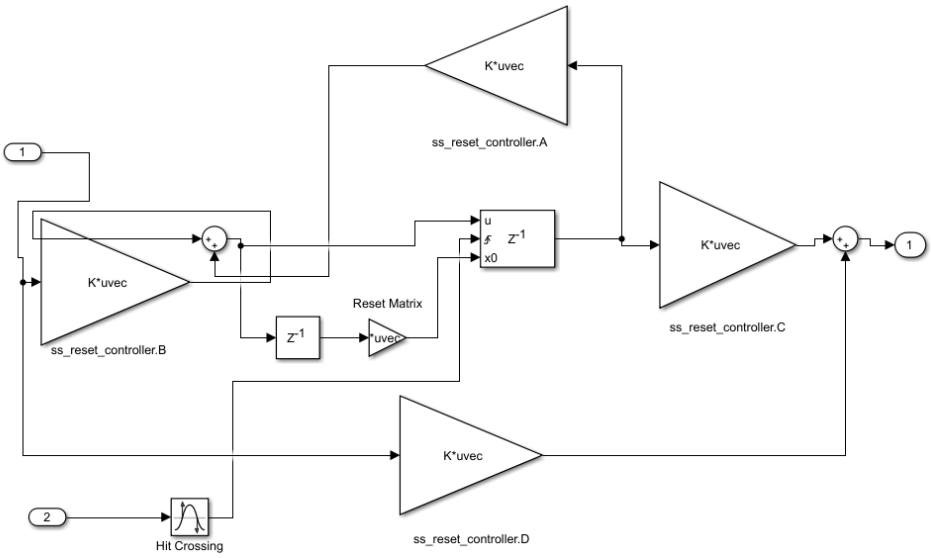

G.10. HOSIDFCALC.M

This function calculates the HOSIDF of a given state space representation for a base linear system given a reset matrix A_ρ

```
function [G] = hosidfcalc(sys, Ar, n, freqs)
    % G = hosidfcalc(SYS, AR, N, FREQS, CLOL)
    % Calculated the higher order (n) describing function for a ...
        reset system.
    %
    % SYS is the reset element described in state space
    % AR is the amount of reset you want to achieve (typical 0)
    % N is the describing function order
    % FREQS contains the frequencies the describing function is ...
        calculated for

    % Kars Heinen - TU Delft - 2018

    % to do; replace inv() by 'matlab \' for faster results

    % odd orders will be skipped
    if (mod(n,2) == 0)
        G = 0;
        return;
    end

    A = sys.a; B = sys.b; C = sys.c; D = sys.d;

    G = zeros(1,numel(freqs)); %this is a vector, which indeed is ...
        the HOSIDF

    for i=1:numel(freqs)
```

```
25          w = freqs(i);
26
27          Lambda = w*w*eye(size(A)) + A^2;
28          LambdaInv = (Lambda)\eye(size(Lambda));
29
30          Delta = eye(size(A)) + expm(A*pi/w);
31          DeltaR = eye(size(A)) + Ar*expm(A*pi/w);
32
33          GammaR = inv(DeltaR)*Ar*Delta*LambdaInv;
34
35          ThetaD = (-2*w*w/pi)*Delta*(GammaR-LambdaInv);
36
37          %Now we calculate the HOSIDF
38          if (n==1)
39              G(i) = C*inv(j*w*eye(size(A)) - A)*(eye(size(A)) + ...
                    j*ThetaD)*B;
40          else
41              % J1 and J2 dissappear
42              G(i) = C*inv(1j*w*n*eye(size(A)) - A)*1j*ThetaD*B;
43          end
44      end
45
46      if (n == 1)
47          G = G + D;
48      end
49  end
```

BIBLIOGRAPHY

[1] Hitachi. *History of Semiconductors*. 2016. URL: https://www.hitachi-hightech.com/global/products/device/semiconductor/history.html (visited on 05/30/2020).

[2] K. J. Åström and T. Hägglund. "The future of PID control". In: *Control Engineering Practice* 9.11 (2001), pp. 1163–1175. ISSN: 09670661. DOI: 10.1016/S0967-0661(01)00062-4.

[3] Linda Chen. "Development of CRONE reset control". PhD thesis. 2017, p. 33. URL: https://repository.tudelft.nl/islandora/object/uuid:5370c610-4112-49e9-b860-9d625d5b40c5?collection=education.

[4] S. Hassan Hosseinnia, Ines Tejado, and Blas M. Vinagre. "Basic properties and stability of fractional-order reset control systems". In: *2013 European Control Conference, ECC 2013*. 2013. ISBN: 9783033039629. DOI: 10.23919/ecc.2013.6669689.

[5] S. Hassan HosseinNia, Inés Tejado, and Blas M. Vinagre. "Fractional-order reset control: Application to a servomotor". In: *Mechatronics* 23.7 (2013), pp. 781–788. ISSN: 09574158. DOI: 10.1016/j.mechatronics.2013.03.005.

[6] Samir Mittal and Chia Hsiang Menq. "Precision motion control of a magnetic suspension actuator using a robust nonlinear compensation scheme". In: *IEEE/ASME Transactions on Mechatronics* (1997). ISSN: 10834435. DOI: 10.1109/3516.653051.

[7] J. C. Clegg. "A nonlinear integrator for servomechanisms". In: *Transactions of the American Institute of Electrical Engineers, Part II: Applications and Industry* (2013). ISSN: 0097-2185. DOI: 10.1109/tai.1958.6367399.

[8] P. W.J.M. Nuij, O. H. Bosgra, and M. Steinbuch. "Higher-order sinusoidal input describing functions for the analysis of non-linear systems with harmonic responses". In: *Mechanical Systems and Signal Processing* 20.8 (2006), pp. 1883–1904. ISSN: 08883270. DOI: 10.1016/j.ymssp.2005.04.006.

[9] Chengwei Cai et al. "The Optimal Sequence for Reset Controllers". 2019. URL: https://www.semanticscholar.org/paper/The-Optimal-Sequence-for-Reset-Controllers-by-Cai-Dastjerdi/ea0ac3b0d2868255e2107699a62b56cfe85b0d58.

[10] A. Oustaloup and M. Bansard. "First generation CRONE control". In: *Proceedings of the IEEE International Conference on Systems, Man and Cybernetics*. 1993. ISBN: 0780309111. DOI: 10.1109/icsmc.1993.384861.

[11] Paul Lambrechts, Matthijs Boerlage, and Maarten Steinbuch. "Trajectory planning and feedforward design for electromechanical motion systems". In: *Control Engineering Practice* 13 (2005), pp. 145–157. ISSN: 09670661. DOI: 10.1016/j.conengprac.2004.02.010.

[12] Orhan Beker et al. “Fundamental properties of reset control systems”. In: *Automatica* 40.6 (2004), pp. 905–915. ISSN: 00051098. DOI: 10.1016/j.automatica.2004.01.004.

[13] Ralph J. Kochenburger. “A Frequency Response Method for Analyzing and Synthesizing Contactor Servomechanisms”. In: *Transactions of the American Institute of Electrical Engineers* 69.1 (1950), pp. 270–284. ISSN: 00963860. DOI: 10.1109/T-AIEE.1950.5060149.

[14] N. M Krylov and N. Bogoliubov. *Introduction to Nonlinear Mechanics*. 1943. ISBN: 0691079854.

[15] Isaac Horowitz and Patrick Rosenbaum. “Non-linear design for cost of feedback reduction in systems with large parameter uncertainty”. In: *International Journal of Control* 21.6 (1975), pp. 977–1001. ISSN: 13665820. DOI: 10.1080/00207177508922051.

[16] Leroy Hazeleger, Marcel Heertjes, and Henk Nijmeijer. “Second-order reset elements for stage control design”. In: *Proceedings of the American Control Conference*. 2016, pp. 2643–2648. ISBN: 9781467386821. DOI: 10.1109/ACC.2016.7525315.

[17] Shih Kang Kuo, Ximin Shan, and Chia Hsiang Menq. “Large travel ultra precision x - y θ motion control of a magnetic-suspension stage”. In: *IEEE/ASME Transactions on Mechatronics* 2.4 (2003), pp. 268–280. ISSN: 10834435. DOI: 10.1109/TMECH.2003.816825.

[18] Robert Munnig Schmidt, Georg Schitter, and Jan van Eijk. *The design of high performance mechatronics*. 2014. ISBN: 9781607508250.

[19] Duarte Valério et al. “Reset control approximates complex order transfer functions”. In: *Nonlinear Dynamics* (2019), pp. 3–4. ISSN: 1573269X. DOI: 10.1007/s11071-019-05130-2.

[20] Kars Heinen. “Frequency analysis of reset systems containing a Clegg integrator”. 2018. URL: https://repository.tudelft.nl/islandora/object/uuid{\%}3Accc37af2-fcbc-46ec-9297-afdc5c1ea4b5.

[21] Antonio Barreiro and Alfonso Bãnos. “Reset control systems”. In: *RIAI - Revista Iberoamericana de Automatica e Informatica Industrial*. 2012. Chap. 1, pp. 11–17. DOI: 10.1016/j.riai.2012.09.007.